

Please fill in your WP specific objectives, progress and impact

1. Explanation of the work carried out by the beneficiaries and Overview of the progress

Explain the work carried out during the reporting period in line with the Annex I to the Grant Agreement.

Include an overview of the project results towards the objective of the action in line with the structure of the Annex I to the Grant Agreement including summary of deliverables and milestones, and a summary of exploitable results and an explanation about how they can/will be exploited¹.

(No page limit per work package but report shall be concise and readable. Any duplication should be avoided).

1.1 Objectives

List the specific objectives for the project as described in section 1.1 of the DoA and described the work carried out during the reporting period towards the achievement of each listed objective. Provide clear and measurable details.

WP8 INSTRUMENTATION - E-TOOLS:

The work of WP8 is three-fold and will further harvest synergies from between the development of

- Task 8.1 New software tools for simulating beamlines from source to detector including estimates of background. The software tools will receive validation input from Task 8.2.
- Task 8.2: Development of innovative shielding concepts and materials for future instruments. The developed concretes will be tested experimentally and performance estimated using the software tools developed in Task 8.1.
- Task 8.3: Development of compact Instrumentation for Larmor Labelling applications at the ESS. The task is developing future instrument concepts that will benefit from both the new simulation possibilities of Task 8.1 and the improved shielding of Task 8.3.

Further, an overall task for all partners is to publish and participate in networking and dissemination of the WP results whenever possible. In the last period, material developed in the WP has been presented at several workshops and meetings.

In connection with the ECNS2019 conference in St. Petersburg, a open, project-wide workshop during presented highlights from the work in all of the WP tasks.

The last period has been very busy for all WP participants, as we have caught up with delayed milestones and deliverables before the end of the project. Hopefully this is reflected in the PR at hand which for WP8 clearly has become the fullest of the three project PRs.

¹ Beneficiaries that have received Union funding, and that plan to exploit the results generated with such funding primarily in third countries not associated with Horizon 2020, should indicate how the Union funding will benefit Europe's overall competitiveness (reciprocity principle), as set out in the grant agreement.

Periodic report template

1.2 Explanation of the work carried per WP

1.2.1 Work Package 8

Explain the work carried out in WP1 during the reporting period giving details of the work carried out by each beneficiary involved.

Milestones MS5 and MS6: ISTSI2019 workshop in St. Petersburg

The original DOW for WP8 defines two separate milestones in the form of workshops on the topics of “Workshop on Larmor concepts for ESS” (MS5) and “Workshop on use of the developed e-Tools for instrument simulation” (MS6).

After discussion in the WP, we however decided that a common workshop would be more attractive as a platform, especially if held in connection with one of the bigger conferences on neutron scattering. As a result, the workshop “Innovative Simulation Tools, Shielding and Instrumentation 2019” (ISTSI2019)² was held in St. Petersburg end of June 2019, as a satellite to the ECNS conference in the first week of July 2019 and delivered a WP-wide platform for dissemination of our activities.

The screenshot shows the homepage of the ISTSI2019 workshop website. At the top left is the SINE2020 logo. To the right is a small image of the ECNS 2019 conference. The main title is "Innovative Simulation Tools, Shielding and Instrumentation 2019 (ISTSI2019)". Below it is the location and date: "Holiday Inn St. Petersburg, Russia, June 29th 2019". A note below states: "- a SINE2020 WP8 "e-tools" satellite event of ECNS2019." Another note says: "The workshop is held as a dissemination activity of the WP8 workpackage in the EU SINE2020 Project and is open to all ECNS2019 participants (registration needed, see below)." The page features a table of speakers and their presentations:

Talk title	Speaker
Welcome and SINE2020 / WP8 introduction	Peter Willendrup, DTU/ESS
News from the RESTRAX/SIMRES project, including MCPL support and McStas bindings for SIMRES	Jan Šaroun, NPI
News from the Vitess project including MCPL support	Egor Vezhlev, FZJ
News from the McStas project, including interoperability solutions for SIMRES, Vitess and MCNP	Peter Willendrup, DTU/ESS
Developments in the MCPL software framework	Thomas Kittelmann, ESS
An optimised neutron super mirror patch for MCNP with applications (ESS-Bilbao)	Esben Klinkby, DTU/ESS
CombLayer-driven MCNP-McStas simulations for simulating instrument signal to noise	Esben Klinkby, DTU/ESS
McStas and Scatter-logger driven calculations of prompt gamma shielding for neutron guides	Rodion Kolevatov, IFE
Studies of relevant design-parameters to enable compact Larmor devices in ESS designs	Katia Pappas, TU Delft
Magnetic field calculations for compact Larmor devices in ESS designs	Michel Thijss, TU Delft
Simulation benchmarks for experiments at the PSI BOA beamline	Erik Knudsen, DTU
Extensions to the Bonner Sphere Spectrometer at PSI, plus experiments and simulation benchmarking for newly developed concrete	Masako Yamada, PSI
Studies of material composition and neutron activation, plus related simulations	Eszter Dian, MTA-EK and Esben Klinkby, DTU/ESS

At the bottom left is the European Union flag, and a note: "This project has received funding from the European Union's Horizon 2020 research and innovation programme under grant agreement No 654000."

Figure 1: Screenshot from the website of the ISTSI2019 workshop website

² See the workshop website at <http://istsi2019.essworkshop.org>

Periodic report template

The total participation to the workshop was 25 attendants, out of which approximately half were not participants of the WP. In total 12 presentations were given, covering all of the WP tasks in simulation software, shielding and Larmor instrumentation.

The presentations from the workshop are available at the ISTSI 2019 website (<http://istsi2019.essworkshop.org>).



Figure 2: A photo of the workshop participants

In the following, we will revisit the progress across the 3 WP8 tasks during the last period, highlighted with graphics and text from the deliverable reports.

Task 8.1: E-tools for integrated simulation using neutronics and Monte Carlo ray-tracing (*Responsible: DTU, Partners: PSI, ESS,NPI, ESS-Bilbao and MTA-EK*)

The task is developing software E-tools for *integrated simulation* using neutronics and Monte Carlo ray-tracing, i.e. will implement and assess new e-science tools for very accurate simulation of neutron beam-lines.

The activity brings together experts from both (a) neutronics, e.g. MCNP used for simulating production and transport of neutrons from the target (including high-energy neutrons and other particles) through moderators and reflectors and (b) Monte Carlo ray-tracing, e.g. McStas and RESTRAX, which in the range of cold and thermal neutrons can describe transport along guides and neutron interaction with other optical elements and samples.

The combination of these two types of code is necessary to allow optimising instruments and experiments from the source to the sample, including shielding. Including shielding allows estimating background, thereby increasing realism of instrument simulations – and for the first time express *instrumental signal to noise* by simulation techniques.

Deliverable 8.8: Port of selected scattering kernels from McStas to SIMRES

The McStas³ distribution contains a large number of components that are used as sample models ranging from very simple benchmarking tools (e.g. Incoherent) to full scale virtual sample-models such as Isotropic Sqw and Single crystal. A full overview list of all included sample models and capabilities is maintained at an ESS-hosted confluence page⁴. This work was intended toward porting the most important/commonly used ones in McStas to SIMRES⁵ to serve both communities. Such a capability could serve two purposes in that it would match the capabilities of SIMRES allowing in some cases to access the backward ray tracing mechanism for speed and still perform accurate simulation with sample models.

In general porting a large code-base to another framework requires careful thought in terms of reliability and maintainability. Simply translating a large piece of code is not considered best practice: as the main development branch evolves and gets updates, the ported code tends to lag behind. It is far better to have an automatic mechanism to transfer code through, or to maintain an solid standard interface between codes. In the case of McStas and SIMRES, the use of MCPL-files⁶ may serve that purpose. This effectively renders all sample-components of McStas available to the SIMRES community all at once.

Interface using McStas instruments and MCPL-files

Figure 3 below shows the minimal McStas-code needed to connect a single crystal, in this case a corundum crystal, to SIMRES. The code simply exposes some parameters of a McStas-crystal to the outside world.

```
1 COMPONENT in = MCPL_input( repeat=1, filename="vin.mcpl" )
2 AT(0,0,0) RELATIVE Origin
3
4 COMPONENT single_crystal = Single_crystal(
5     reflections="Al2O3_sapphire.lau",
6     yheight=0.05, radius=0.01, mosaic=1, delta_d_d=1e-4,
7     az=4.757, ay=0, az=0, bx=2.3785, by=0, bz=-3.364,
8     cx=0, cy=12.9877, cz=0,
9     p_transmit=0.1)
10 AT (0, 0, 0) RELATIVE PREVIOUS
11
12 COMPONENT out = MCPL_output( filename="vout.mcpl" )
13 AT(0,0,0) RELATIVE PREVIOUS
```

Figure 3: Listing of minimal McStas sample instrument, with a Sapphire single crystal as scattering element. In principle the sample description can be any McStas instrument - that can thus be integrated into SIMRES.

Method summary

In summary, the developed simulation pipeline, from a user perspective, is:

1. Define the primary spectrometer in SIMRES
2. Define the secondary spectrometer in SIMRES

³ See the McStas website at <http://www.mestas.org> and the shared McStas/McXtrace GitHub repository at <https://github.com/McStasMcXtrace/McCode>

⁴ See <https://confluence.esss.lu.se/display/MCSTAS/McStas+sample+model+functionality-matrix>

⁵ See the RESTRAX/SIMRES website at <http://neutron.ujf.cas.cz/restrax/> and the publication <https://doi.org/10.1016/j.nima.2010.06.219>

⁶ Monte Carlo Particle List (MCPL) format, see <https://doi.org/10.1016/j.cpc.2017.04.012>, <https://mctools.github.io/mcpl/>, and SINE2020 deliverable report D8.2

3. Set parameters for the sample scattering kernel in a minimal McStas-file, and compile it.
4. In sequence:
 - a) run primary spectrometer,
 - b) run minimal McStas sample
 - c) run secondary spectrometer.

This procedure effectively “ports” all available McStas sample kernels to SIMRES in one go, and keeps the operating modalities of both simulation programs with no additional maintenance effort.

Ready-made ports of selected samples

To further illustrate the possibilities and ease of use of McStas samples from within SIMRES (or other codes supporting the MCPL format), a subset of the McStas sample components have been wrapped in the same type of instrument file as illustrated in Figure 3. For standardization purposes all of the instrument files take input from an MCPL file named similarly to the instrument file and give output with a similar naming scheme, i.e.

`McStas_[sample]_in.mcpl → McStas_[sample].instr
→McStas_[sample]_out.mcpl`

The finalized set of interface-instruments developed for use with SIMRES are

- `McStas_PowderN.instr` for interfacing the standard McStas powder model
- `McStas_Single_crystal.instr` for interfacing the standard McStas single crystal model
- `McStas_Isotropic_Sqw.instr` for interfacing the standard McStas liquid/“isotropic material” elastic-inelastic model

For more information, please refer to the SINE2020 Deliverable 8.8 report.

Deliverable 8.11: Improved user interface

The title of this the D8.11 report is “Improved user interface”, but should not be taken too literally - we are not as such developing user interfaces to the expert codes that the work in WP8 is based on. Rather, we have focused on:

- a) providing worked and documented examples and use-cases and examples of expert codes.
- b) developing interfaces between expert codes.

This way we maximize output from the work package and provide long term maintainable tools for users. In practice we are providing the users with an interface to all of our developed software solutions and methods to date, facilitated by a new GitHub repository with example datasets and thorough documentation at <https://github.com/McStasMcXtrace/SINE2020WP8>.

The developed solutions

The most easily applicable product of our WP is the MCPL event interchange software (see D8.2), for which support has been implemented in several softwares (see D8.2, D8.8 and D8.18) and used to solve a number of WP tasks (see D8.4, D8.1 and D8.13).

Supplementing the nice documentation readily available for MCPL (see <https://mctools.github.io/mcpl/> and the related open access publication⁷), we have decided to make a number of practical examples of the use of MCPL available through our WP GitHub repository at <https://github.com/McStasMcXtrace/SINE2020WP8>.

⁷ Kittelmann, T., Klinkby, E. B., Bergbäck Knudsen, E., Willendrup, P. K., Cai, X. X., & Kanaki, K. (2017). Monte Carlo Particle Lists: MCPL. Computer Physics Communications, 218, 17-42.

<https://doi.org/10.1016/j.cpc.2017.04.012>

Softwares supporting MCPL usage

Since the 2016 release of MCPL, a number of softwares currently support event exchange, see below Figure 4, reproduced by the ISTSI2019 presentation by Thomas Kittelmann, ESS.

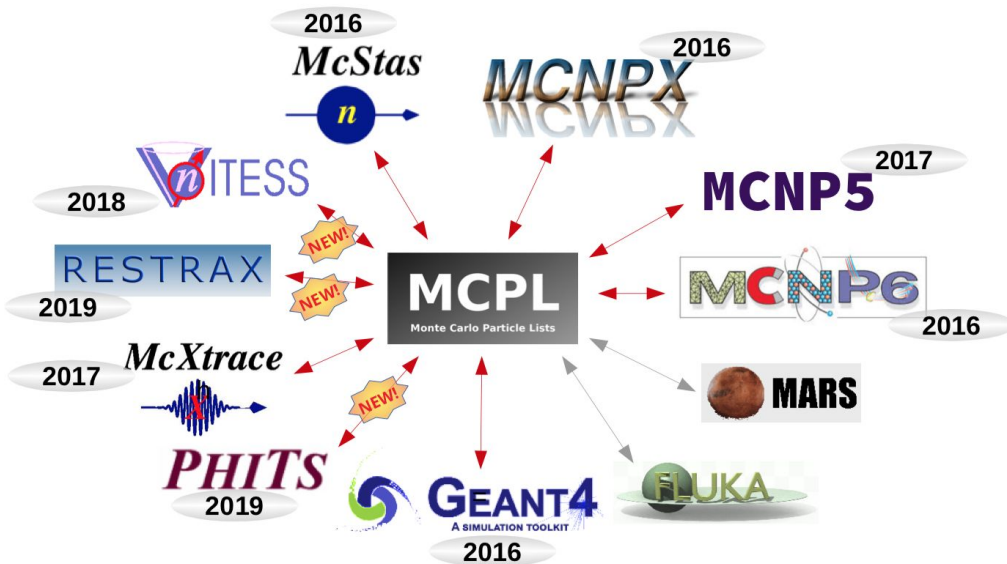


Figure 4: Current overview of softwares with MCPL bindings

MCPL usage examples

In the section below we will highlight a number of MCPL usage examples, to illustrate the flexibility and versatility of the MCPL solutions:

MCPL example 1) MCNP-based ESS source terms for use with McStas.

In connection with the assessment of the effect of new ESS source characteristics on instrument performance, a series of MCNP calculations were done for most of the ESS beamlines. The output in each case was an MCPL file containing individual neutron (and gamma etc.) events reaching a given beamport (as illustrated in Figure 5). These beamport-files have been made available through a dedicated website at the ESS DMSC:

<http://public.esss.dk/users/willend/MCPL/>. Together with the McStas template instrument ESS_butterfly_MCPL_test.instr which has been distributed with McStas since release 2.4.1 (2016), the simulated MCNP neutron events can be transported along neutron guides in the McStas software.

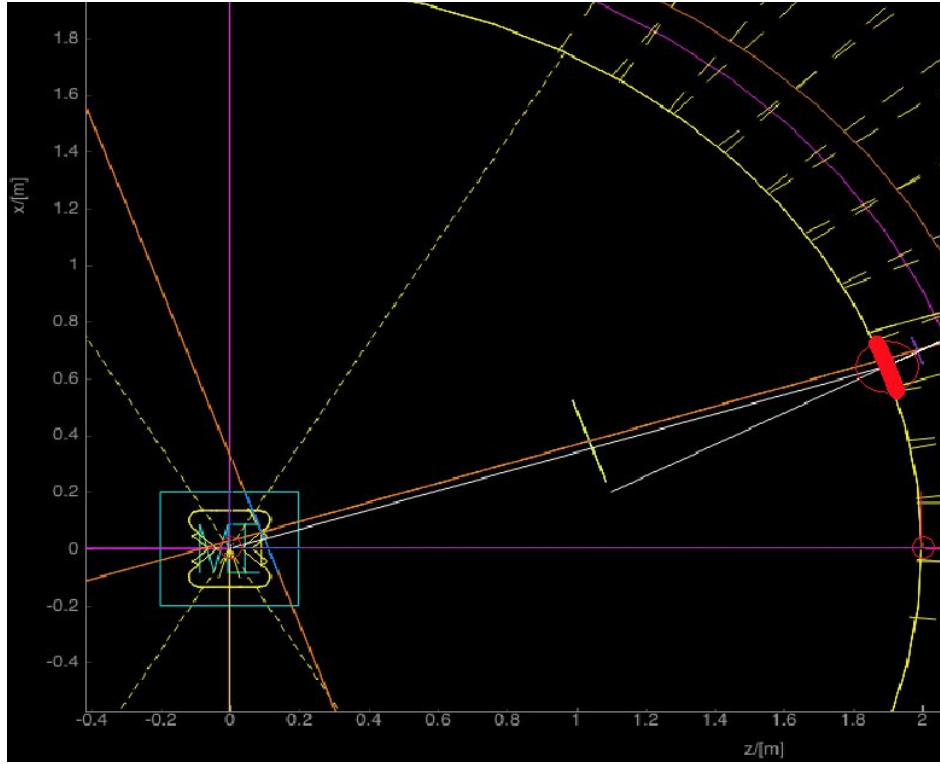


Figure 5: Visualisation of events in the file `W8.mcpl.gz` within the `ESS_butterfly_MCPL` instrument. The coordinate system of choice is the `TARGET` coordinate system.

To ensure agreement with analytical models of the ESS moderators available in McStas, neutrons transported through a simple curved neutron guide on beamport W8, using both the analytical and MCPL-based ESS source models. As can be seen when comparing Figure 6 and Figure 7, the agreement is very good.

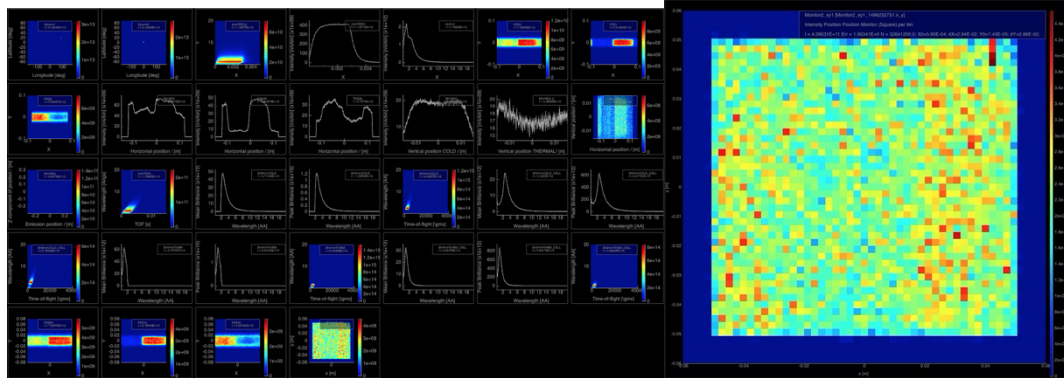


Figure 6: Output from the MCPL source: - overview plot and "end of curved guide" PSD for the W8 beamline.

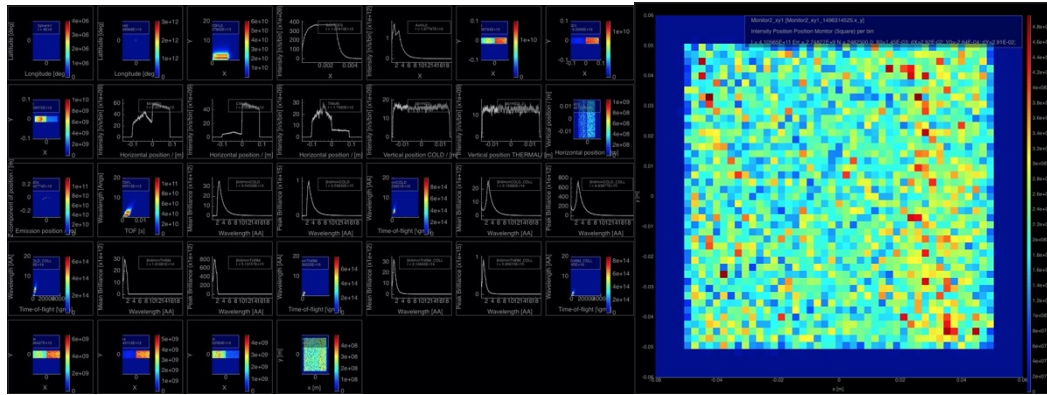


Figure 7: Output from the analytical ESS source: - overview plot and "end of curved guide" PSD for the W8 beamline.

As an example of use of this methodology outside of WP8, we refer to deliverable report D8.11 where we show how the same approach has been used at ORNL for describing new source terms for the renovated HIFR reactor.

MCPL example 2) Geant4-based detector model used with McStas input data.

In connection with detector developments for the LoKI SANS beamline at ESS, MCPL files were used for transferring output from a McStas model of the beamline, including a simulated sample to a realistic Geant4 model of the detector. contains figures reproduced from which is referred to for further details.

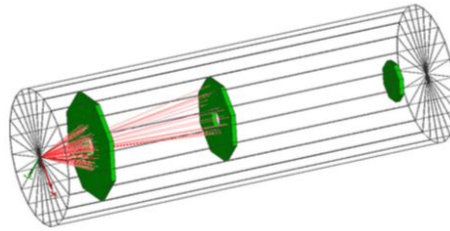


Figure 8: Geant4 model of a complex, hexagonal detector originally envisioned for the LoKI instrument. Neutrons from the sample hitting the active detector area appear in red.

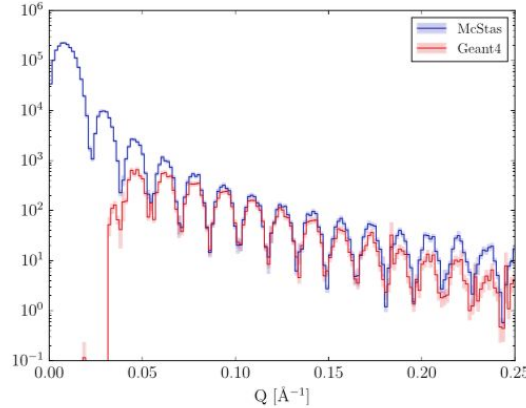


Figure 9: Raw Q distribution for a subset of the LoKI detectors (middle detector bank shown right). The McStas post-sample output appears in blue, while the distribution calculated from the simulated measurements in Geant4 appears in red.

MCPL example 3) Transfer of functionality from McStas to Vitess.

MCPL was further applied in to enable users of the Vitess software⁸ to work with updated models of the ESS source from McStas, as Vitess was at the time (2017) not considered actively

⁸ See https://www.helmholtz-berlin.de/forschung/oe/em/transport-phenomena/neutronmethods/vitess/index_en.html

Periodic report template

developed. In this solution, the general mcstas2vitess script was used to create Vitess modules containing MCPL_input.comp, MCPL_output.comp and ESS_butterfly.comp from McStas. Full details of the solution can be found at a dedicated ESS Confluence page⁹.

Luckily Vitess has since revitalised by the employment of Klaus Lieutenant at FZ Jülich, and since v. 3.4 of Vitess, the software now readily includes all of the above functionality.

MCPL example 4) SIMRES-McStas Simulations of the BEER instrument.

An advanced example is included with the newly released SIMRES version 6.4.0[5] based on the proposed BEER instrument at ESS. IN this example:

1. The primary spectrometer is simulated using a reverse Monte Carlo procedure in SIMRES.
2. The sample (a powder) is simulated with McStas
3. The secondary spectrometer using a forward Monte Carlo process is traced in SIMRES.

In between steps 1,2, and 3 is an interface layer of simple intermediary MCPL-files. This advanced example is striking for several reasons: 1) for its use of reverse Monte Carlo which in cases like this may speed calculations up by O(3). 2). for its automated interfacing to McStas, through the mechanism developed in D8.8 . Lastly the combination is completely automated to run within the SIMRES regular user interface as shown below.

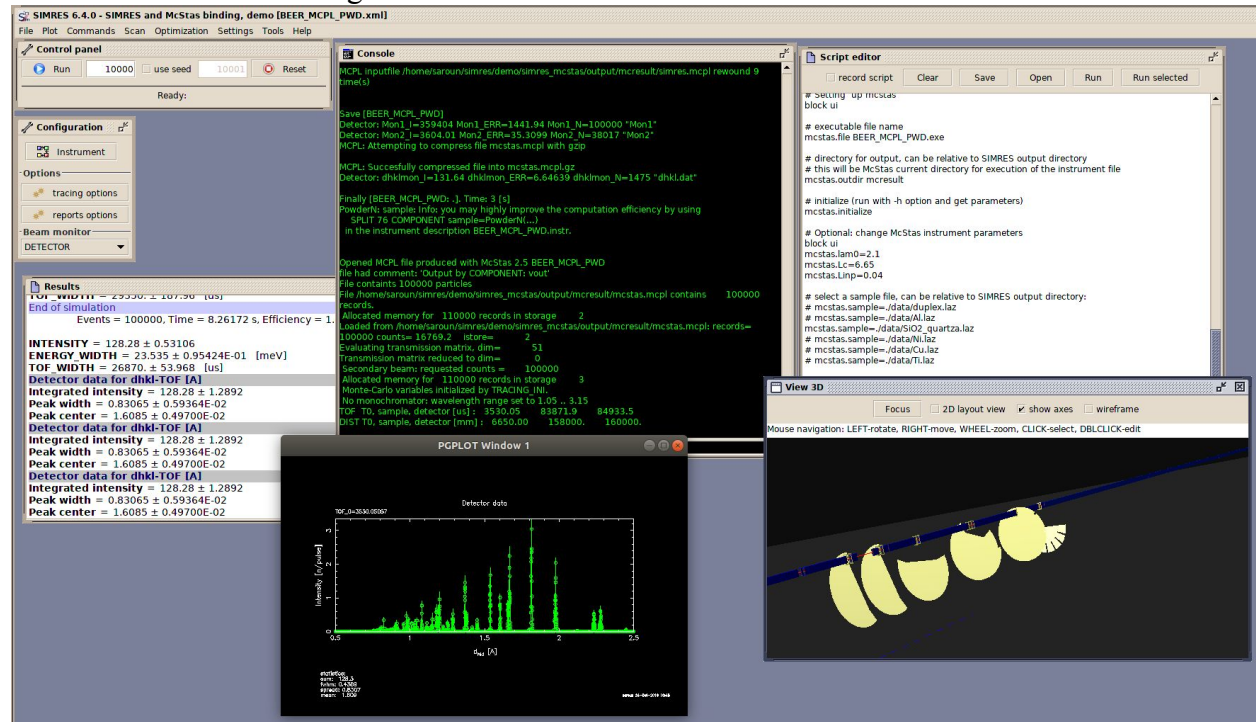


Figure 10: The main SIMRES window when running McStas simulation as a part of the ray-tracing process.

Running the simulation as described in section 6 in the SIMRES user manual[5], results in a powder diffraction signal as:

⁹ See <https://confluence.esss.lu.se/pages/viewpage.action?pageId=238390110>

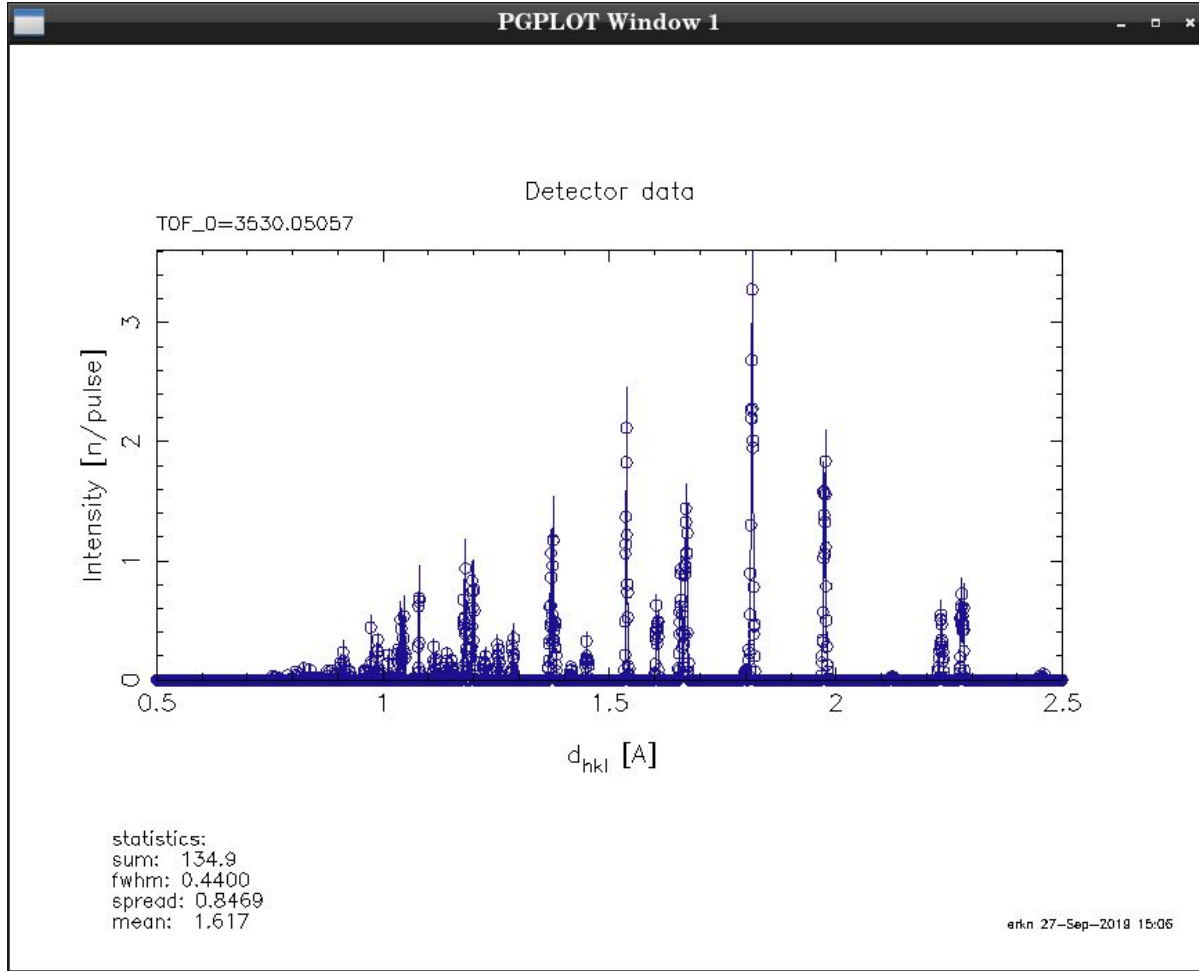


Figure 11: Neutron scattering signal from a duplex steel powder sample, simulated by the SIMRES-McStas-SIMRES pipeline developed in WP8.

Importantly, we note that these simulation required < 1 min complete runtime on a standard laptop computer. Not bad, considering that this may be seen as a simulation of complete instrument!

MCPL example 5) Scatter logger with MCPL

This example shows how to use the Scatter logger interface to McStas to extract information about neutron intensity lost in the walls of a neutron guide. In this case the definition of *lost* is intensity that is *not reflected* at the guide wall surface. This is important to keep in mind. McStas in general treats reflectivity phenomenologically as something that happens on the mirror surface plan - i.e. there is no distinction of which surface layers reflect what (and at what depth) in a suppermirror setting [6].

As a very simple first example of such use - we here plot the escape vectors for the first 2000 neutron events for a standard m=1, 10 m straight guide which is illuminated by a 5 Å neutron source with 1% bandwidth. For clarity we have scaled the velocity vectors' length by 1/1000.

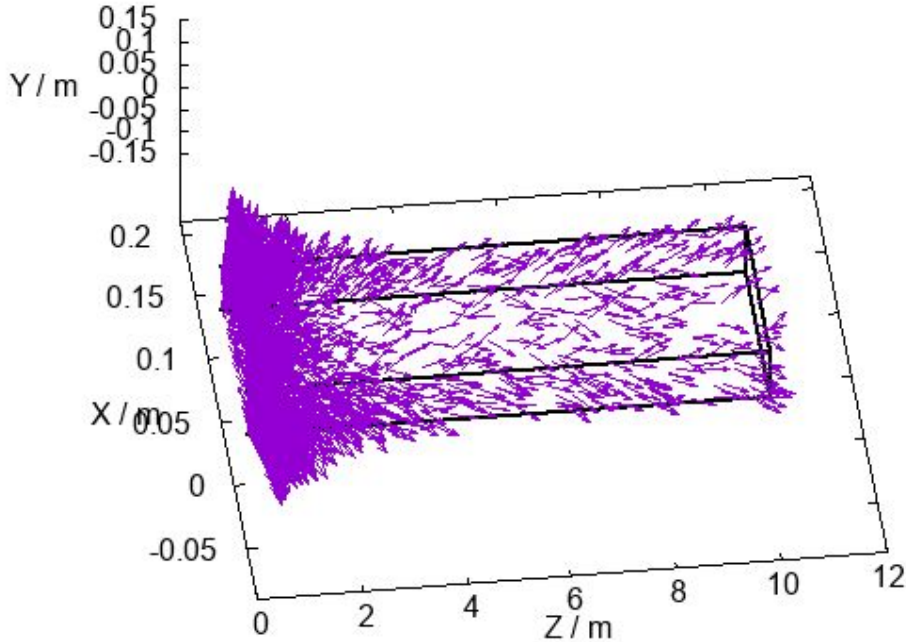


Figure 12: Velocity vectors of neutron events that escape a straight 10 m guide, at the points where the guided rays are reflected in the guide supermirrors.

Some care needs to be taken when interpreting this kind of plot as it does not directly correspond to the lost intensity, merely the statistical events which may be processed further to reveal what intensity is lost where. The simulation calculates the point along the guide where a neutron ray is reflected and with what intensity lost. These data points are logged and later revisited to generate a set of neutron rays which is saved to an MCPL-file. Such events can then further be processed using dedicated software to provide a handle on for instance shielding characteristics. Recent results developed by R. Kolevatov^{10,11} show that such data can be transformed into gamma ray generation estimates in realistic guide settings.

Deliverable 8.12: Software documentation and report on combined RESTRAX + McStas simulations

The possibility to combine capabilities of two ray-tracing programs, McStas and RESTRAX, in one simulation were exploited within the task 8.12. Utilities allowing to redirect ray-tracing process to/from McStas simulation have been developed in SIMRES (the ray tracing program from the RESTRAX project). The method builds on the Monte Carlo Particle Lists format library (MCPL), which enables binding of the programs without extra costs for porting codes and

¹⁰ Kolevatov, R., Neutron absorption in supermirror coatings, Journal of Neutron Research, 2012

¹¹ Kolevatov, R., McStas and Scatter Logger driven calculations of prompt gamma shielding for the neutron guides, Journal of Neutron Research, in review.

Periodic report template

maintenance of interfaces. The development chains and working environments of both the programs can therefore remain completely independent. Report D8.12 documents the method and shows four use examples, where this technique brings substantial benefits to users, including large improvement of simulation speed and the possibility to employ a wider choice of component models by both programs. Beamline configurations which could not be simulated so far by either of the programs due to the lack of suitable components or simulation speed become thus feasible.

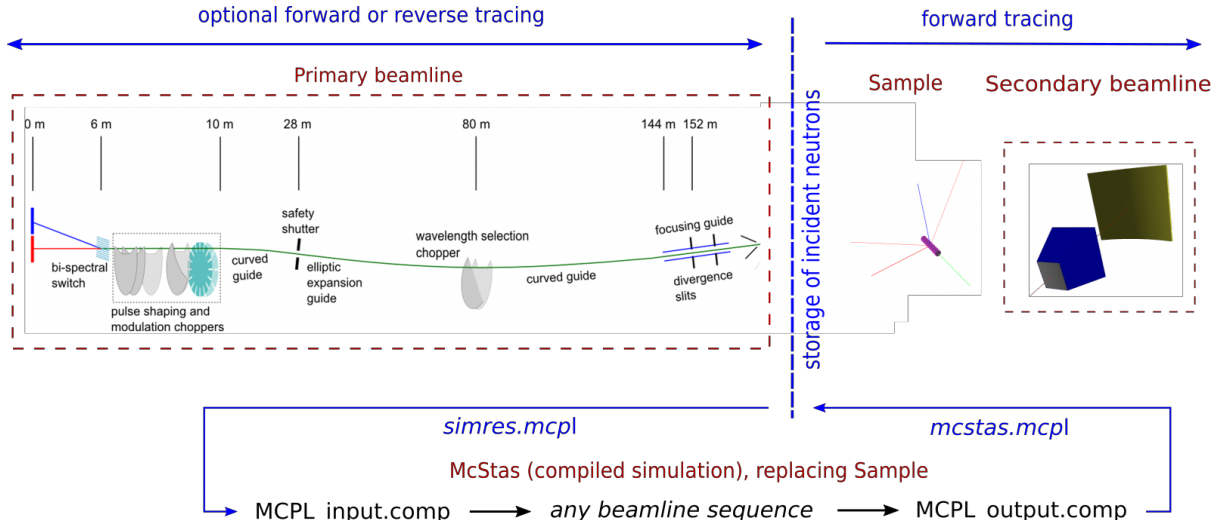


Figure 13: A schematic showing the flow simulation when combining SIMRES and McStas, from D8.12.

As it turns out, the combination of SIMRES back-tracing of the primary beam path and the McStas sample model in the secondary beam path is both fast and accurate. See Figure 14 and Table 1 below.

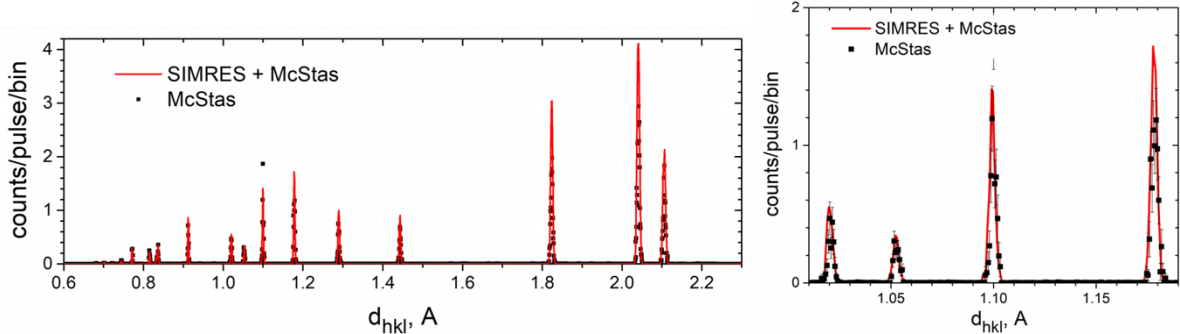


Figure 14: Diffractograms simulated by the combined SIMRES+McStas ray-tracing (red line) and by McStas only (black points). The detail on the right permits to assess differences, which are within the statistical errors.

Table 1. Comparison of computing times and statistical errors for the primary beam intensity.

Simulation setup	Rel. error (primary beam)	Computing time
SIMRES+McStas	1.1%	56s
McStas	1.8%	1110s

BEER in modulation mode

The combination of SIMRES and McStas tracing described above has also been applied to test event based data reduction procedure for strain measurements in beam modulation mode of BEER. In this mode, the primary beam is modulated by a fast chopper with multiple windows, placed close to the source. As a result, a chain of several diffraction lines is measured by the detector for each diffracting plane. Whereas SIMRES enables fast simulation of the primary beam even with the small gauge volume required for strain mapping, McStas enables to easily implement new or derived component models. The detector component NPI_toft_dhkl_detector.comp has been developed for data reduction of the modulated data. It permits to reconstruct single high-resolution diffraction lines from the modulated pattern, which have higher peak intensity compared to the usual pulse shaping mode with similar resolution. In this example, the primary beam has been simulated by SIMRES in reverse tracing direction, while the sample (PowderN.comp) followed by the radial collimator and detector was simulated in McStas. The modulation chopper MCB rotating at 280 Hz, with $8 \times 4^\circ$ slits was used to modulate the beam. The gauge volume of $1 \times 1 \times 2 \text{ mm}^3$ was defined by a primary slit and secondary radial collimator similarly to the previously mentioned simulation. The sample was again a duplex steel rod of 7 mm diameter oriented with the axis parallel to the mean diffraction vector (45° orientation).

In Figure 15, the wavelength-time maps of neutrons at the sample (SIMERS output) and detector (McStas output) are shown. The diffractograms produced by the McStas detector are then plotted in Figure 16.

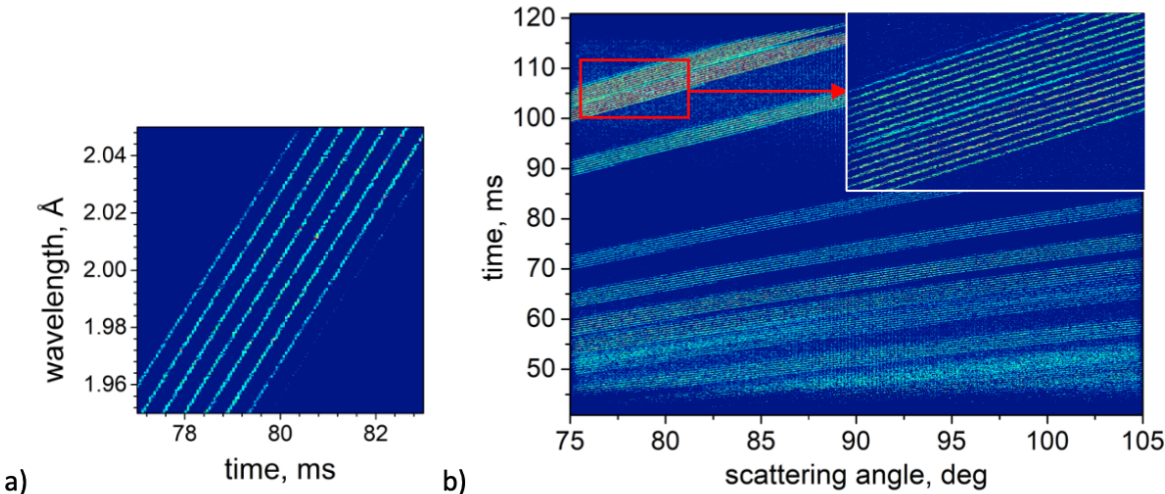


Figure 15: a): Modulated beam structure at the primary slit – SIMRES MCPL output passed to McStas. b): TOF- 2θ map of events registered by the detector component (NPI_toft_theta_monitor.comp) in McStas; multiplexed diffraction lines from the duplex steel sample (PowderN.comp)

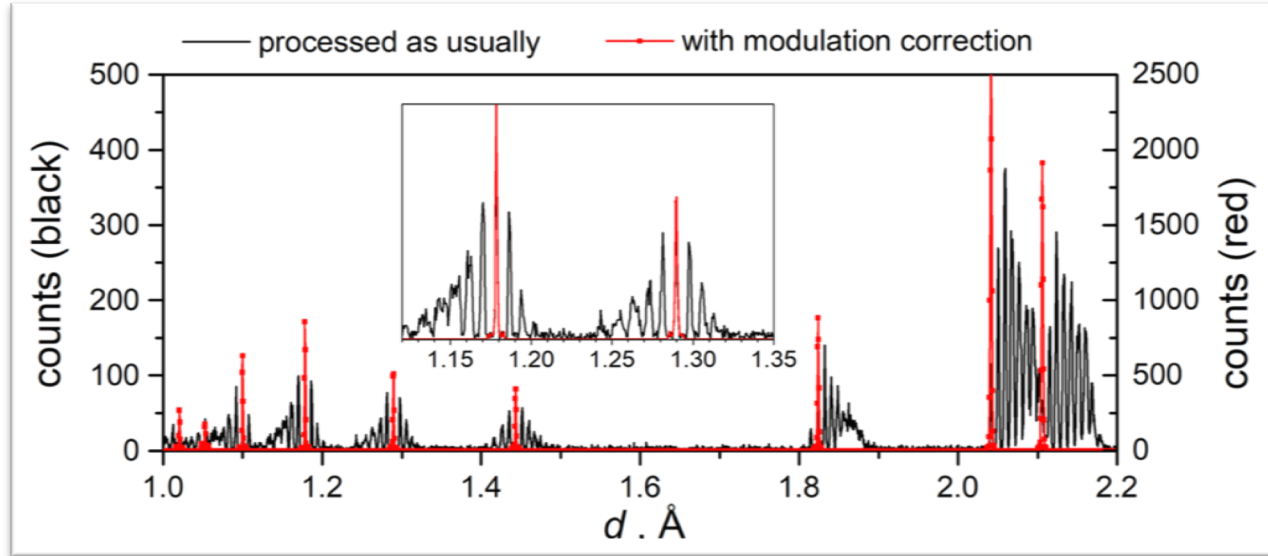


Figure 16: Diffractogram produced by the McStas component NPI_tof_dhkl_detector with the modulation analysis switched off (black, left scale) and on (red, right scale).

Single crystal diffraction in BEER

To test the variety of scattering models in McStas, the BEER instrument was simulated with a single crystal sample (Single_crystal.comp) in white beam mode (Laue diffraction). This configuration used following settings:

- **Choppers:** switched off (white beam).
- **Wavelength bandwidth:** from 0.5 Å to 2.7 Å.
- **Primary collimation:** divergence slit 15x15 mm (6 m before the sample), primary slit 4x4 mm² placed at 50 mm before the sample axis.
- **Sample:** a-SiO₂ cube 3x3x3mm³, mosaicity 30° (data file SiO₂_quartz.lau)
- **Detectors:** cylindrical (PSDcyl_monitor) and 4PI (PSD_monitor_4PI) monitors, and 1x1m² 3He detector at 90° (PSD_Detector).

As before, the primary beam was simulated by SIMRES, ray-tracing through the sample was performed by McStas. Scattered beam monitors were defined in both McStas and SIMRES. Note that the wide cylindrical detector is not part of the BEER project and this simulation serves merely as a demonstration of bringing new scattering models to SIMRES via MCPL event

exchange. The simulated scattering pattern as detected by SIMRES detector is shown in

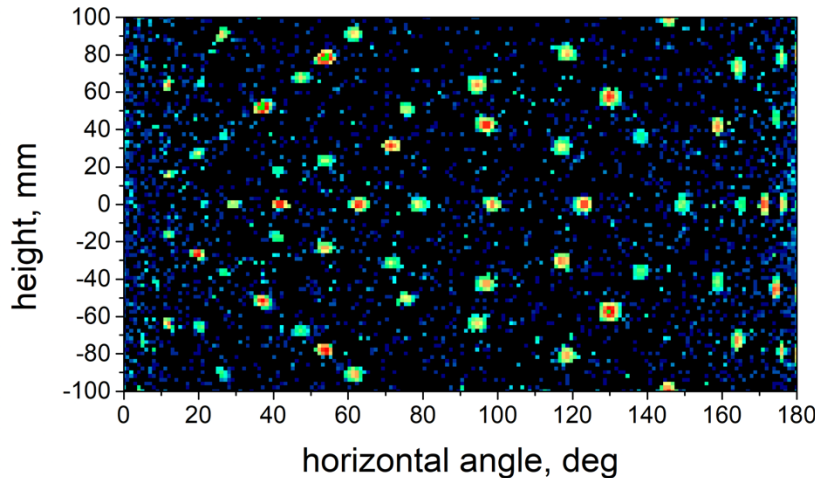


Figure 17: Single crystal diffraction pattern ($\alpha\text{-SiO}_2$) recorded by the SIMRES detector. The primary beam was simulated by SIMRES. Simulation of the sample was redirected to McStas. The secondary beam was traced by both McStas and SIMRES.

Simultaneous diffraction and SANS measurement at BEER

Unlike the previous example, simultaneous measurement of diffraction and small-angle scattering belongs to the scope of the BEER project, assuming installation of a SANS detector as a part of the ESS completion program. The chopper system of BEER permits to operate the instrument in the so called alternating wavelength frame mode, when the sample is exposed alternatively to thermal neutrons in one source period, followed by cold neutrons in the next period. The bandwidth in both ranges is limited to about 1.75 \AA , while the mean wavelengths of the thermal and cold beams are separated by 3.5 \AA .

Although there is no component in McStas or SIMRES which combines diffraction and SANS scattering models, it was rather easy to extend the existing component PowderN so that it handles SANS in addition to diffraction and incoherent scattering. The simplest case of monodisperse spheres was used for demonstration. Results of this simulation are summarized in below, please refer to deliverable report D8.12 for further details.

Periodic report template

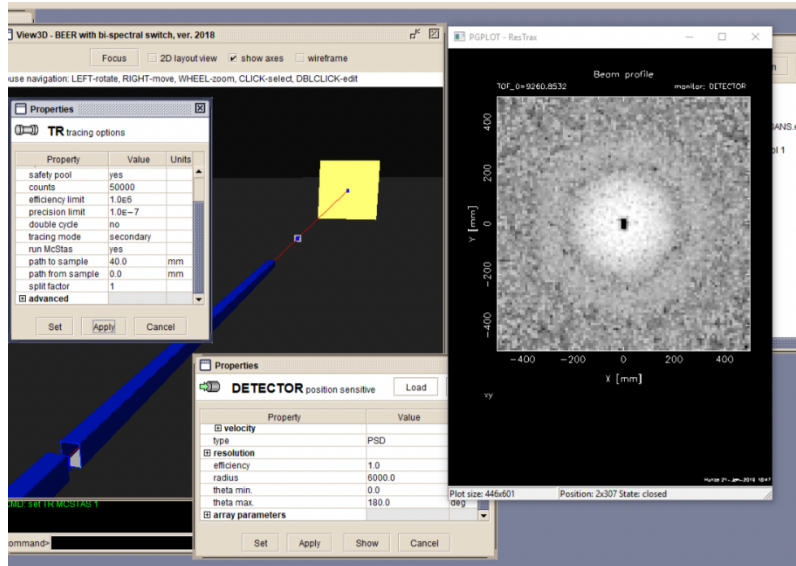


Figure 18: screenshot of the SANS pattern shown in the SIMRES user environment. Primary and secondary beams were simulated by SIMRES. Simulation of the sample was redirected to McStas.

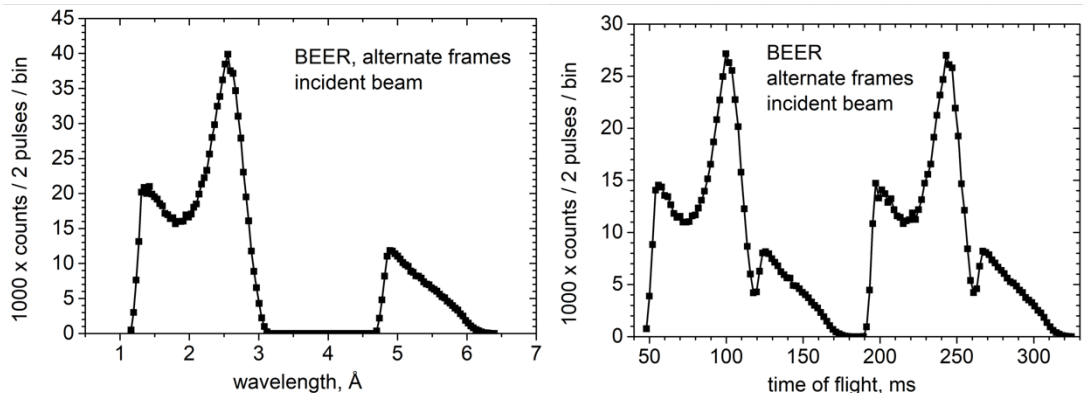


Figure 19: Time structure (left) and spectrum (right) of the primary beam simulated by SIMRES for BEER in the alternating frame mode. It was used as MCPL input to the subsequent McStas simulation of the sample and secondary beamline, see also Figure 20

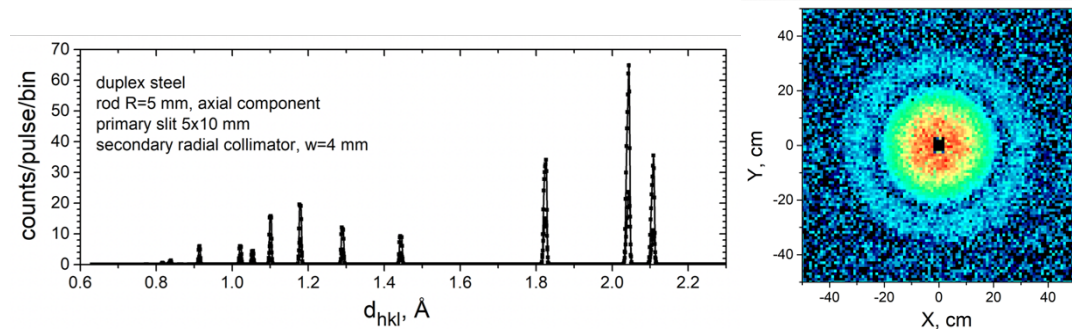


Figure 20: Diffractogram and SANS pattern ‘measured’ simultaneously on the same sample - output of the McStas simulation of the secondary beam.

Deliverable 8.13: Optimization study of a selected instrument using CombLayer and McStas-MCNPX

This deliverable report D8.13 “Optimization study of a selected instrument using CombLayer and McStas-MCNPX” presents simulations to assess the expected **sample-position** signal-to-noise for the future BIFROST instrument at the European Spallation Source. For these simulations, we compare a palette of software and solutions developed in SINE2020 WP8. To the extent possible, the used codes and models have been made available through the SINE2020WP8 GitHub repository at <https://github.com/McStasMcXtrace/SINE2020WP8>

The instrument and selected tools:

To assess the capabilities of the various coupling schemes developed, the BIFROST instrument at ESS was chosen. The reasoning behind this choice is that BIFROST is a long instrument (150m) and makes use of elliptical guides and therefore ranks among the most challenging instruments to model at the ESS.

The main tools applied in this study are

- Comblayer to drive the generation of the main BIFROST MCNP deck
- MCNP-variants
 - MCNP6.2 including the latest supermirror-patch (see also deliverable report D8.3)
 - Standard MCNPX/CINDER for activation-induced gamma production
- McStas v. 2.5
- MCPL for transfer events between MCNP variants and McStas
- Geometrical validation through co-visualisation of engineering CAD-drawing and McStas model
- McStas-based shielding logger from Rodion Kolevatov (IFE) to estimate neutron capture along the BIFROST optics

Comparison of Super-Mirror enabled MCNP (SM-MCNP) and MCPL-McStas method

Based on the Comblayer (http://coimbra2016.essworkshop.org/slides/CombLayer_Ansell.pdf) implementation of the BIFROST instrument an MCNP inputfile is prepared as illustrated in Figure 21 below. Several manual adjustments of the model were required, see deliverable report D8.13 for details.

As an alternative modelling approach to the MCNP-only solution, a coupled MCNP McStas simulation was carried out. As in the above, MCNP proton on target simulations constitute the first step. Rather than deriving a dedicated beamline specific MCNP source at the guide entrance, the neutrons are simply handed to McStas, through the recently developed MCPL interface^v. This coupling allows the individual neutron state parameters as determined at a given surface in MCNP to be stored on disk and used as a source in a subsequent McStas simulation. A comparison between the lost intensity along the beamline in the two model descriptions was then carried out. As can be seen in Figure 22 below, the agreement between the two methods is not perfect, but at least of the same order of magnitude.

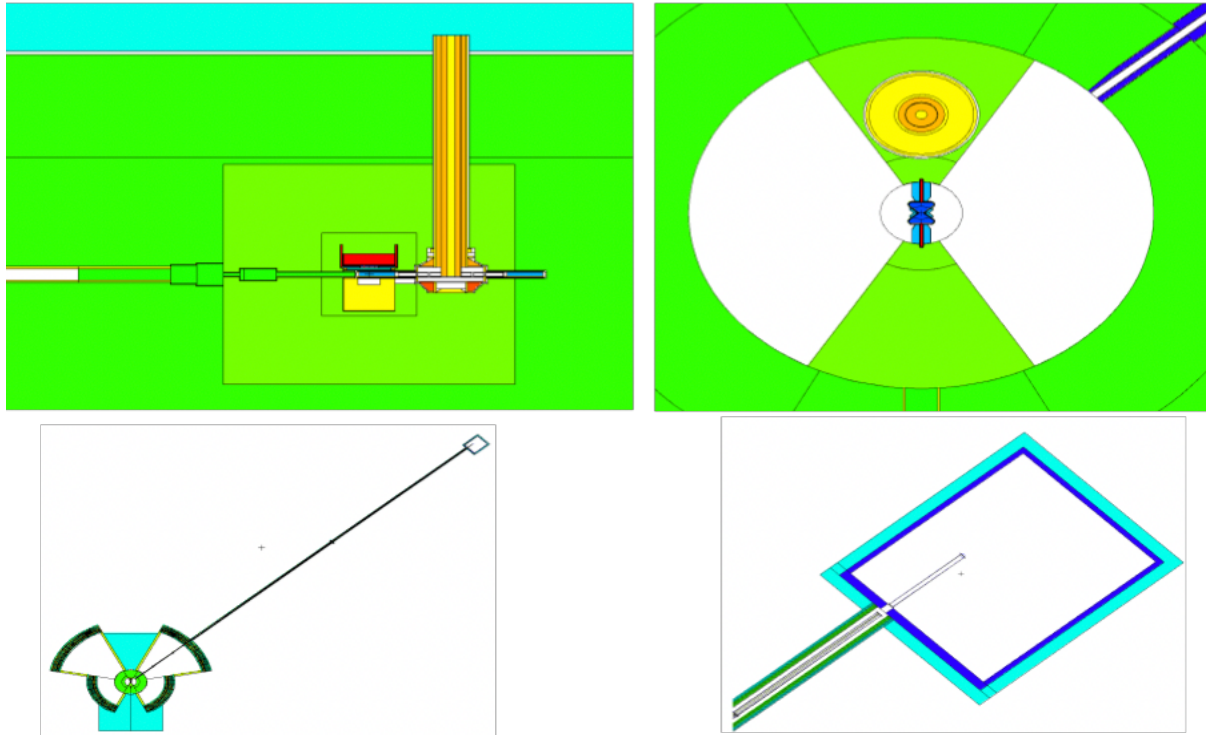


Figure 21: Top left: protons arriving from left - the illustration shows the target (horizontal disk) and target shaft (vertical, orange) as well as the moderator-reflector plug (central, red+yellow). All is encapsulated in steel (green) for shielding purposes. Top right: cross-section through the central parts of the ESS, showing the (blue) butterfly shaped moderator. Lower left: birds perspective of the facility, showing the target building and bunker as well as the BIFROST guide and instrument cave. Lower right: BIFROST Instrument cave.

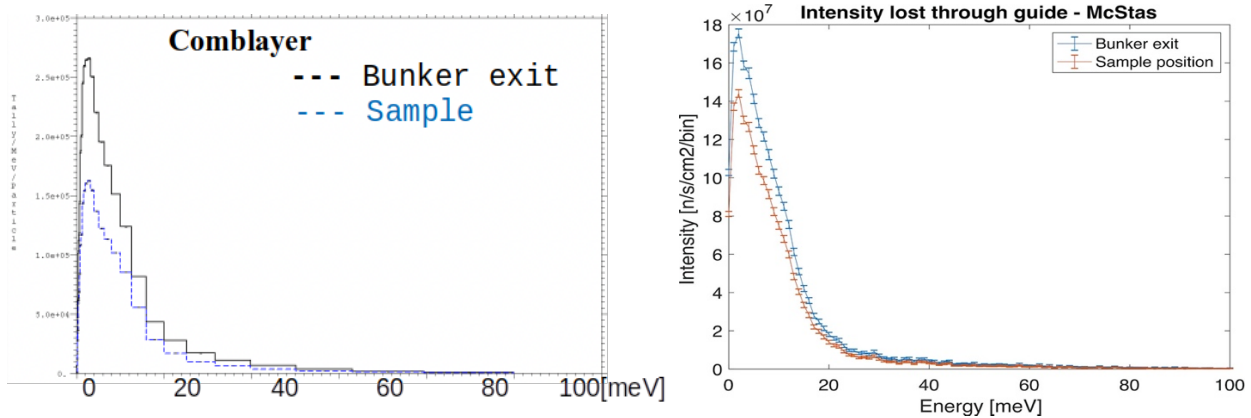


Figure 22: Left: The spectrum at the sample position, and at the bunker exit. The intensity loss during the 150m transport amounts to 37% (0-100meV). Right: Neutron energy spectrum at the bunker exit (blue) and at the sample position (red) using a MCNP-McStas coupled simulation. The intensity loss in the McStas simulation is 22%

Geometrical model-validation

The Comblayer/MCNP model was based on engineering drawings from the ESS. The McStas model however originated from a GuideBot¹² model, which was manually adjusted and gave input to the engineering model. Hence it was necessary to ensure geometrical agreement between e.g. the engineering model and the McStas model. Thus, the engineering CAD drawing in CATIA format was first converted to STL1 and finally to OFF2 format which can be read and visualised in McStas. The figure below shows a good agreement (of order a few cm over the 150 m) between engineering CAD model and McStas model.

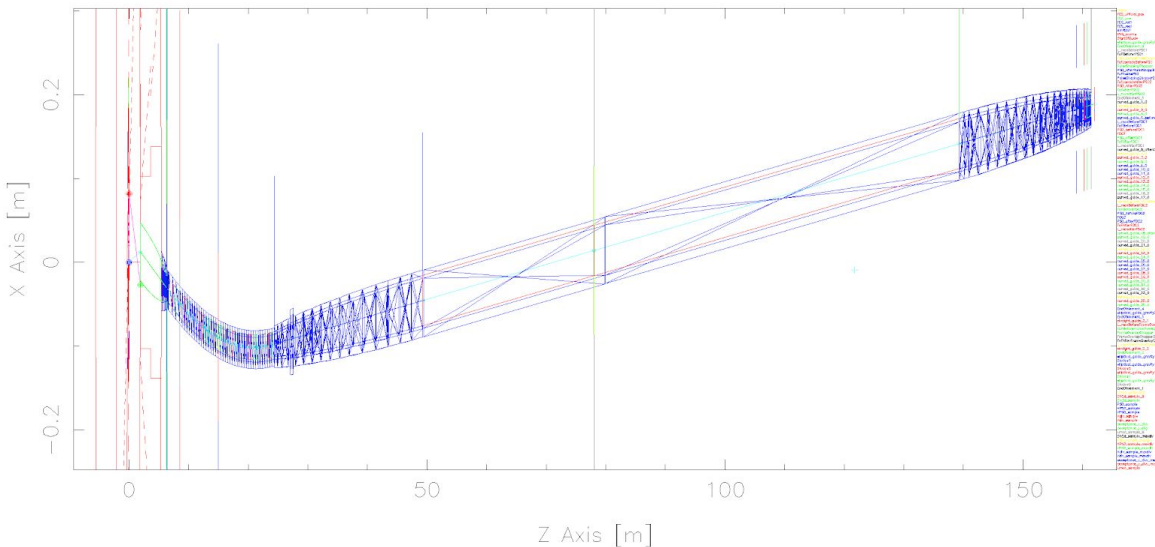


Figure 23: CAD model (blue) overlayed with McStas instrument geometry. The precision in placement of the sample position is of the order cm over the 150 m instrument length.

Gamma-production estimates through Shielding logger

Dr. Rodion Kolevatov from IFE has not been directly involved with the SINE2020 WP8 work, but has been working on shielding aspects of BIFROST as part of the Norwegian in-kind involvement with ESS. In connection with this work, Dr. Kolevatov has devised a method¹³ to estimate gamma-production in supermirror-coatings, resulting radiation dose-rates and needed shielding. The method is based on processing the ‘lost’ intensity in McStas, that is the non-reflected portion of the neutron beam, and uses the principle of the so-called scatter logger¹³.

Dr. Kolevatov contributed a presentation to the SIN2020 WP8 workshop *ISTSI2019*, and announced the availability of easy-to-use McStas-based components implementing the abovementioned method, and we hence found it natural to mention this development in the context of our related deliverable report. The figures below are reproduced from his forthcoming publication^x.

¹² Bertelsen, M 2017, 'The automatic neutron guide optimizer guide_bot', Nuclear Instruments and Methods in Physics Research Section A: Accelerators, Spectrometers, Detectors and Associated Equipment, vol. 867, pp. 195-203. <https://doi.org/10.1016/j.nima.2017.06.012>

¹³ E. B. Knudsen, P. K. Willendrup, E. B. Klinkby, McStas event logger : Definition and applications, Nuclear Instruments and Methods in Physics Research Section A: Accelerators, Spectrometers, Detectors and Associated Equipment — 2014, Volume 738, pp. 20-24 <https://doi.org/10.1016/j.nima.2013.11.071>

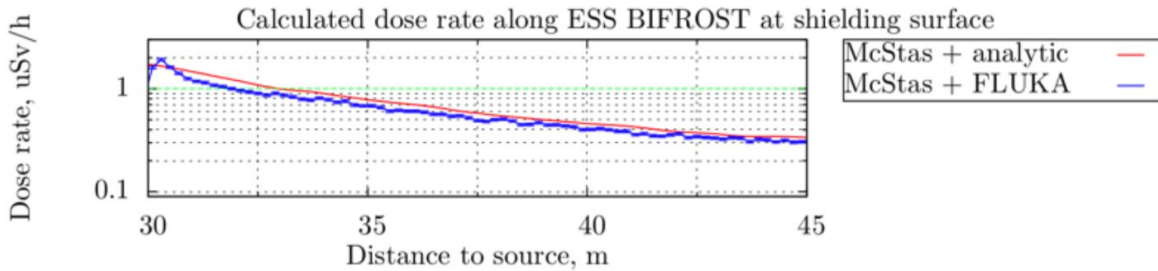


Figure 24: Dose rate along ESS BIFROST guide shielding at the surface calculated according to reference ix and using FLUKA

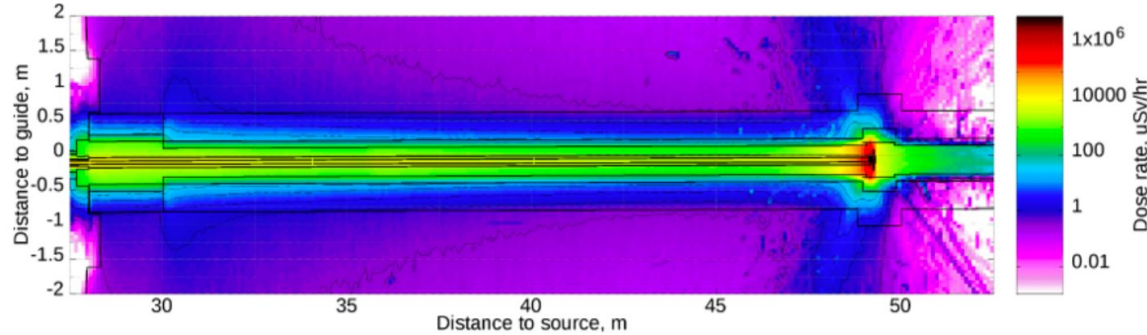


Figure 25: Dose rate distribution in the shielding around BIFROST guide, cut by horizontal plane at guide height.

Deliverable 8.18: Comparative Vitess & MCNP simulations

Introduction

The goal of collecting the escaping neutrons and produced prompt gamma yield during the Monte Carlo simulation of a neutron scattering instrument is to help the calculation of the realistic dose rate around the instrument, thus to increase the accuracy of the shielding calculations.

The program packages written for Monte-Carlo modelling of the neutron scattering instruments can only calculate the transport of the thermal or cold neutrons. Other Monte Carlo codes like MCNP or Geant 4 can calculate the transport in the matter of many particles having wide energy ranges. These codes generally cannot take into account the coherent scattering of neutrons i.e. the reflection of the thermal and cold neutrons, and their absorption yield in the reflection coating. The neutron supermirror is a multilayer structure consisting of some hundred to some ten thousand nickel and titanium layers. The neutron is reflected either by total reflection on the top Ni layer or via Bragg reflection on the deeper layers. The Bragg reflection can be described only by using dynamical scattering theory, that means that the neutron absorption in the reflective layer cannot be calculated using simple geometrical considerations. A general linearized conservative (that overestimates the dose rate) calculation however, can be found in the work of Rodion Kolevatov^{ix}.

The aim of the D8.18 work was to modify the Vitess (Virtual Instrumentation Tool for the European Spallation Source) program package to calculate and store the gamma photons produced by the neutrons in the reflective layer of the neutron guides due to prompt gamma activation.

Vitess^{vi} is built to simulate neutron scattering instruments using the Monte-Carlo ray tracing technique. Its philosophy is to provide a user friendly simple tool for building modular virtual instrument. That means that there are predefined neutron optical elements - like sources, neutron guides, monochromators, spin polarizers etc. - with predefined input- and output variables. The

components are written in C, but - not like in McStas - they are compiled during the installation i.e. the package is modular and flexible, but the components cannot be changed without changing the source code and recompiling the component.

In an earlier work¹⁴ by the D8.18 authors, the prompt gamma yield was calculated by an external program applying geometrical considerations using the position, direction and wavelength values of the reflected and non reflected neutrons.

There are two ways to produce the gamma source file:

1. Collection of the gamma photon and escaping neutron yield on the mirror segments, and production of a source term with the averaged spectra of photons and neutrons like in the earlier work.
2. Collection of the particles in an MCPL^v file as an input for other Monte-Carlo codes.

Since the first version works only for one program package amongst the programs able to calculate shielding properties, we chose the second version.

Results

In order to register the gamma yield arising from absorption of neutrons in the coating we changed the source code of the guide component (guide_parallel.c written for parallelized calculation of the neutron transport in neutron guides).

We extended the component by:

- Calculation of the prompt gamma lines during reflection using the linearized conservative calculation of Rodion Kolevatov[4]
- Storing of the produced photons and neutrons escaping from the guide in MCPL structure[3]
- Saving the result in an MCPL file that works as input for Monte-Carlo based program packages used for shielding calculations.

To check the code we simulated a neutron bender which is a curved neutron guide designed for fast curving of the neutron beam. The bender has many neutron channel to have many thin neutron guides enabling the curvature with small radius. Both walls of the channels are coated with neutron supermirror. The material of the wall is thin borofloat glass containing 12 mass % of natural boron. The borofloat substrate does not absorb all of the neutrons due to its width and the scattering of the glass, but the neutrons reaching the substrate have such direction that make them impossible to be reflected on the other reflecting layers. Thus the absorption and the scattering in the other layers and substrates can be calculated by applying geometrical considerations i.e. the escaping neutrons can be handled by other Monte-Carlo programs. In Figure 26 the spatial distribution of the prompt gamma yield is visible projected to different planes, where both the coating, and the decreasing intensity of the beam – the decreased reflection density - is visible. In Figure 27 the gamma spectrum is shown binned in 17 different energy bins.

¹⁴ A. Szakál et. al. “Optimization of focusing supermirror neutron guides for low γ -background”, Nuclear Instruments and Methods in Physics Research Section A Accelerators Spectrometers Detectors and Associated Equipment 2011, 634(1) pp S130-S133 <https://doi.org/10.1016/j.nima.2010.06.007>

Periodic report template

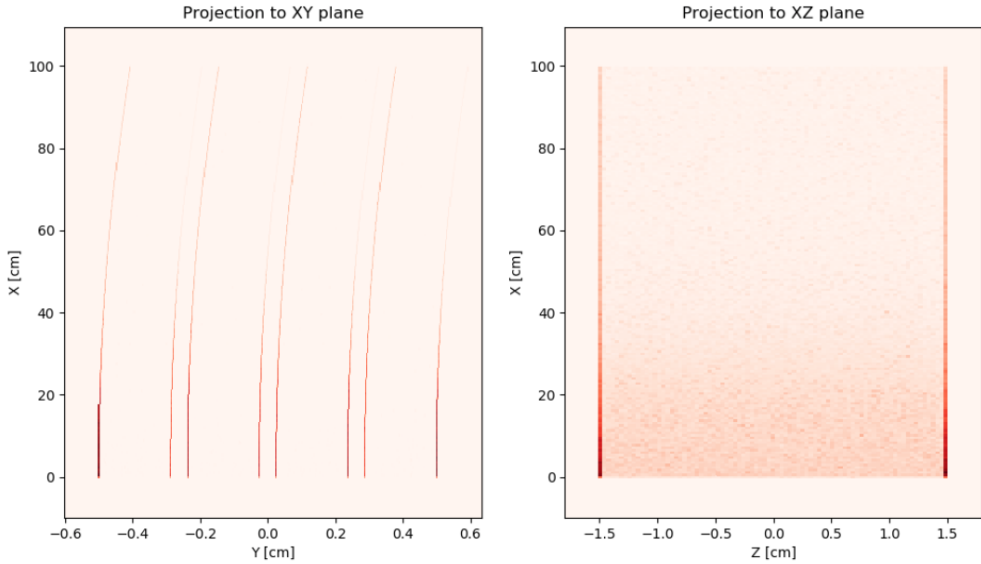


Figure 26: Gamma production yield projected to the horizontal plane (left) and the vertical plane parallel to the incident beam direction.

In Figure 26 the spatial distribution of the gamma production rate is visible. On the left side the coating on the substrate is clearly visible. At the beginning many neutrons got lost due to the high divergence of the neutrons. Later there are larger rate on the outer planes due to the larger reflection angles. On the right side the gamma absorption on the top and bottom plane is clearly visible together with the decreasing of the absorption as the function of the flight path. The increased yield at the walls is due to the projection i.e. the top and bottom walls are parallel with the projection direction.

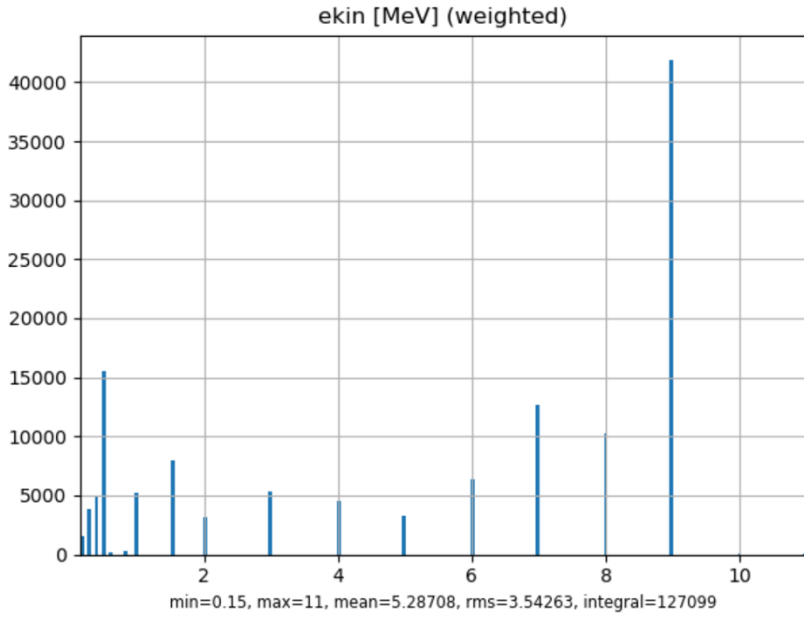


Figure 27: Gamma energy distribution due to prompt gamma absorption in the reflective layer.

In Figure 27 the binned energy distribution of the gamma yield is seen. Instead of the real gamma lines the intensities are collected in 17 energy bins. This solution decreases the number of particles in the MCPL file while stays conservative since the upper limit of the bins are given

Periodic report template

as energy values. The high energy lines of Ni and Ti are strong showing that the prompt gamma activation of the reflective mirror can have significant part of the dose rate outside the shielding because the half length of the concrete for the half MeV gamma photons arised from absorption of boron is 3-4 times smaller than the half length for the high energy gamma photons. For further details, please refer to deliverable report D8.18.

Deliverable 8.20: Final release of all software

Software and methods developed within the SINE2020 WP8 collaboration have been made available at a dedicated GitHub repository with example datasets and documentation at <https://github.com/McStasMcXtrace/SINE2020WP8>.

The screenshot shows the GitHub repository page for 'McStasMcXtrace / SINE2020WP8'. The repository has 6 issues, 0 pull requests, 0 projects, 0 wiki pages, 0 security vulnerabilities, 0 insights, and 0 contributors. It contains 82 commits, 1 branch, and 0 releases. The latest commit was by user 'willend' on 9 days ago. The repository description is 'Repository for software and methods developed in WP8 under the EU SINE2020 project'. The README.md file is visible at the bottom.

Repository for software and methods developed in WP8 under the EU SINE2020 project

Manage topics

82 commits 1 branch 0 releases 2 contributors

Branch: master New pull request Create new file Upload files Find file Clone or download

Author	Commit Message	Date
willend	Update README.md	Latest commit 8c033e8 9 days ago
Deliverable-reports	Add last deliverable from Budapest	16 days ago
Publications	Update README.md	9 days ago
Workshops	Add links to workshop websites	23 days ago
code	Update README.md	18 days ago
examples	adding readme for activation	23 days ago
images	Adding banner	8 months ago
patches	Update README.md	16 days ago
README.md	Update README.md	14 days ago

README.md

SINE2020WP8

Repository for software and methods developed in WP8 under the EU SINE2020 project

This project has received funding from the European Union's Horizon 2020 research and innovation programme under grant agreement No 654000

For more information, please visit the SINE2020 website at <https://www.sine2020.eu>

Unless explicitly noted, all software and examples in this repository is licensed under [GPL v2.0](#).

Other files and documentation are licensed under [Creative Commons Attribution-NonCommercial-ShareAlike 4.0 International License](#)

Figure 28: Front page of the GitHub repository, with clearly visible license terms.

The page gives easy access to

- PDF versions of deliverable reports
- Links to the WP8 workshops held during SINE2020
- Links to repositories and webpages of the used softwares
- Example datasets and simulation input files

- An overview of related publications

All WP8 partners have been encouraged to put copies of useful files or data in the repository for future use and dissemination purposes.

Task 8.2: Innovative Shielding Concepts and Materials (Responsible: PSI,

Partners: ESS, STFC, ESS-Bilbao, TUM, MTA-EK and DTU)

The main focus of Task 8.2 in WP8 is the research into new concrete mixes and the optimisation of laminate shielding structures, including the development of heavy concrete mixes or comparable materials, for effective shielding of neutrons is spear-headed by the PSI.

Deliverable 8.10: Several background measurement series at different facilities in Europe

Introduction:

Simulating complex spallation source setups related to background is time-consuming and it is connected with uncertainties. That's why neutron spectra measurements are very important for the optimisation of neutron scattering instruments. The goal of the task was to perform a series of background measurements at facilities in Europe.

The Neutron detector system used:

The SINE2020 WP8 developed BSS-System was used to measure at first the neutronic background at SINQ@PSI (Switzerland) and secondly at AKR-2@TU Dresden (Germany).

Figure 29 shows the used detector and moderator spheres.



Figure 29: New BSS-system with PE moderators and Cu shells

Facility study 1: SINQ Neutron Bunker

The neutron guide bunker at SINQ/PSI was chosen to perform most of the background measurements because the guide bunker offers ideal conditions for measurement. The bunker can be accessed during beam development time of SINQ (every three weeks) and it was known that a significant fast neutron spectrum can be measured. Figure 30 shows the neutron guide bunker layout including the measurement positions.

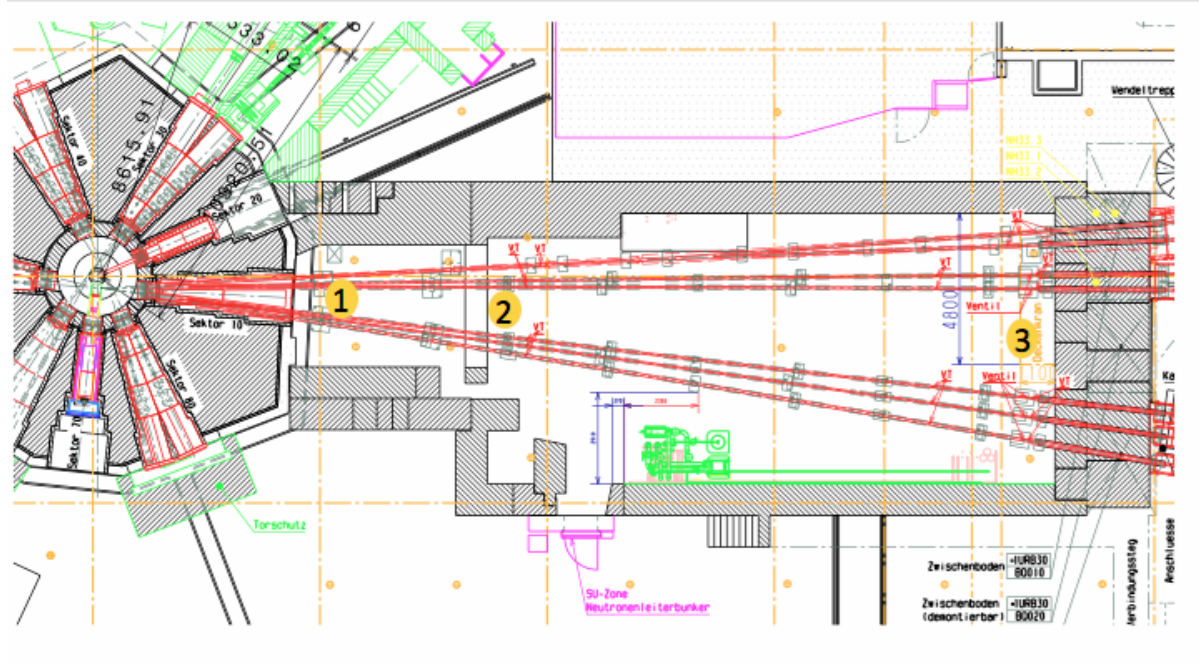


Figure 30: SINQ neutron guide bunker with the three measurement positions

In total 3 different position were chosen to measure the background. The first position is very closed to the target. The distance is approximately 6m. The second position (see Figure 31) was chosen because the neutron guide bunker is divided into two sections. The sections are also physically separated by a 70 cm thick concrete wall. The distance to the target is 12 m.

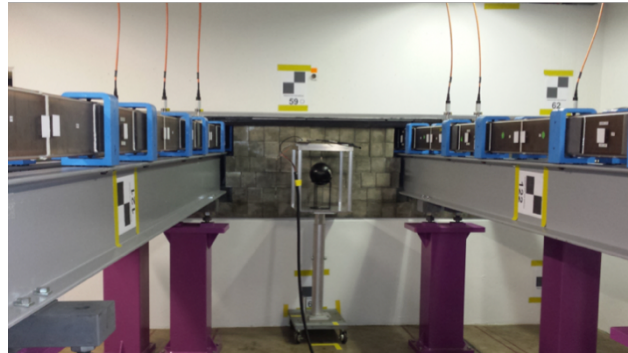


Figure 31: Setup in the middle position 2

The third position is at the end of neutron guide bunker. The neutron scattering instruments are located behind the last shielding wall.

Facility study 2: AKR-2 Reactor

The AKR-2 reactor was chosen as the second neutron facility where background measurements can be done. Also the facility in Dresden offers good conditions to measure the fast neutron spectra. The detector system can be positioned around 1.5m away from the reactor core. In both cases, position A as well as position B, direct view to the reactor core is given (see Figure 32).

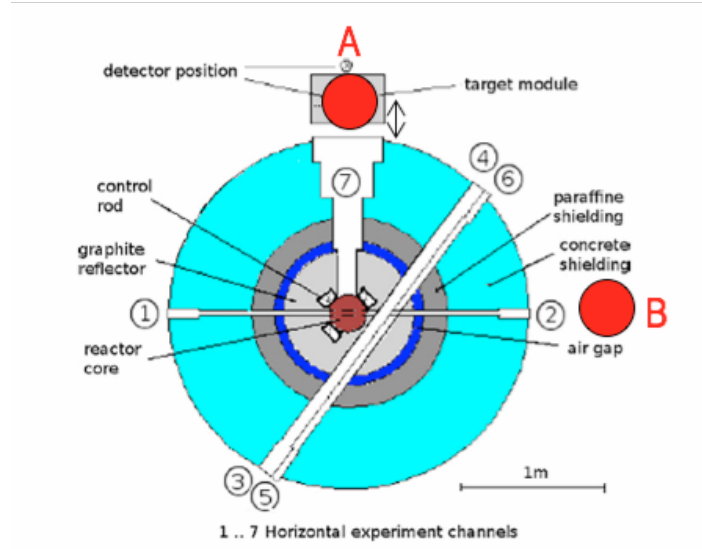


Figure 32: Cross section of the reactor setup and the two measurement positions

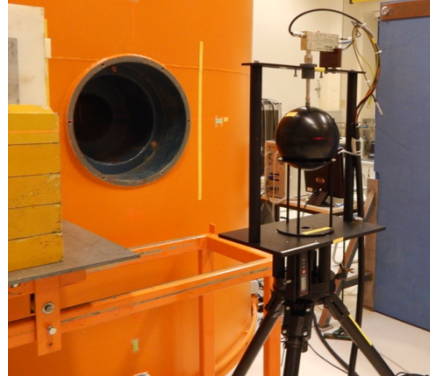


Figure 33: Measurement setup at position A

Especially position A can be used for the BSS measurements because the opening (see Figure 33) has a dimension of around 48 cm in diameter. The biggest BSS sphere is 30 cm in diameter. The detector setup was positioned to the central coordinates of the beam port.

Results for facility 1, SINQ neutron guide bunker

In Figure 34 below we show the results of the measurements in the SINQ neutron guide bunker. In addition MCNPX simulations for position 1 were done to cross check the results.

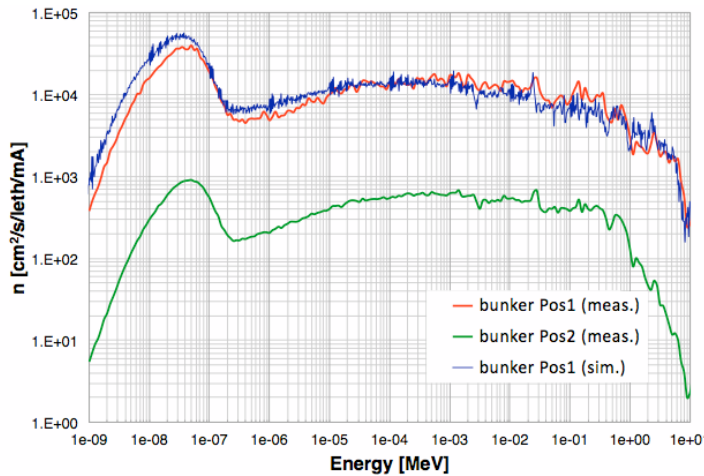


Figure 34: Neutron spectra for Position 1 and 2 in the SINQ neutron guide bunker

The measurements were done outside of the neutron beam but the data are showing a strong contribution in the thermal region. The fast part of the spectra has few resonances which can be explained by the cross section resonances of iron. At SINQ the main shielding is realized by iron.

The agreement between simulations and measurement is very good. The small differences in the thermal region could be scattering effects which are not fully implemented in the MCNPX model.

Please consult deliverable report D8.10 for further details.

Results for facility 2, : AKR-2 Reactor

The BSS detector system is mainly developed to measure neutron spectra in homogenous fields. Otherwise it need response function corrections. For that reason neutron imaging was done at the AKR-2 in Dresden. Figure 35 shows the thermal neutron distribution of measurement position A. The image was combined by 9 separate measurements because the field of view of the detector is only 100 mm x 100 mm. The conclusion was that the standard BSS data treatment can be used because the beam is homogenous enough. The centre image was used for normalization.

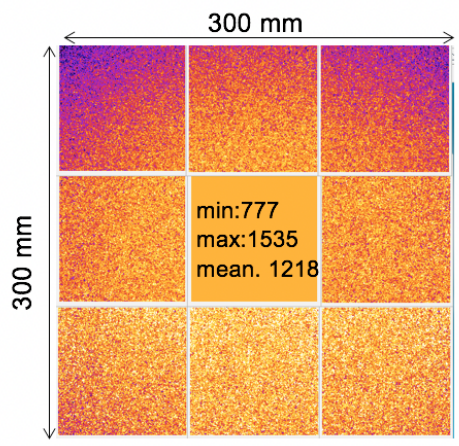


Figure 35: Thermal Neutron flux distribution of AKR2 position A

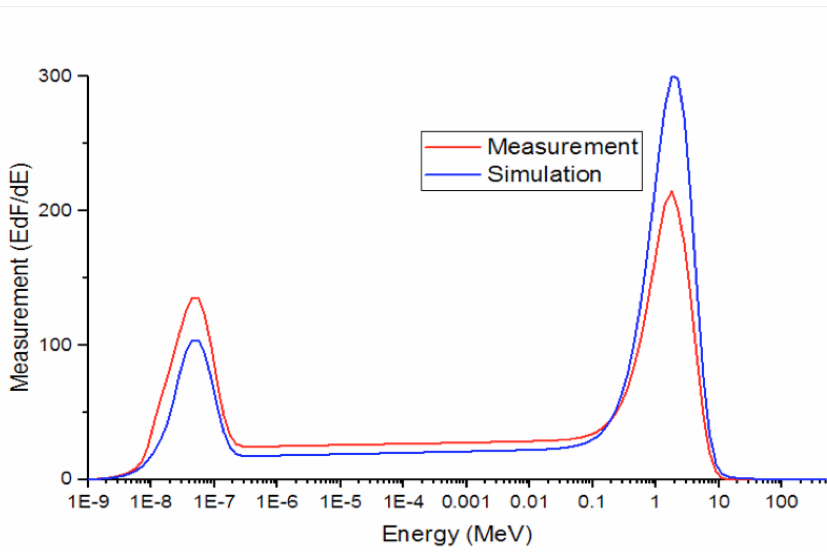


Figure 36: Measurements and Simulations for Position A

The data evaluation for the AKR facility is shown in Figure 36. A dominant fast neutron spectrum was measured where the fast neutron region is higher as the thermal part of the spectrum. The additional MCNP simulation confirmed the measurement and shows the even higher fast neutron peak at 2 MeV. The spectrum can be explained that most of the released neutrons are not moderated in the core.

Deliverable 8.14: Investigation of effective shielding concepts for high energy particles

Simulating complex spallation source setups related to background is time-consuming and it is connected with uncertainties. The goal of the task was to investigate effective shielding setups by measurements at the PSI BOA beamline.

As mentioned already under Deliverable D8.10, a BSS-System was developed and within this task used to investigate effective shielding setups. Please consult Figure 29 again for a look at the used detector and moderator spheres.

The experimental setup

The beamline BOA at PSI was chosen to investigate different material setups. Figure 37 below shows the beamline layout.

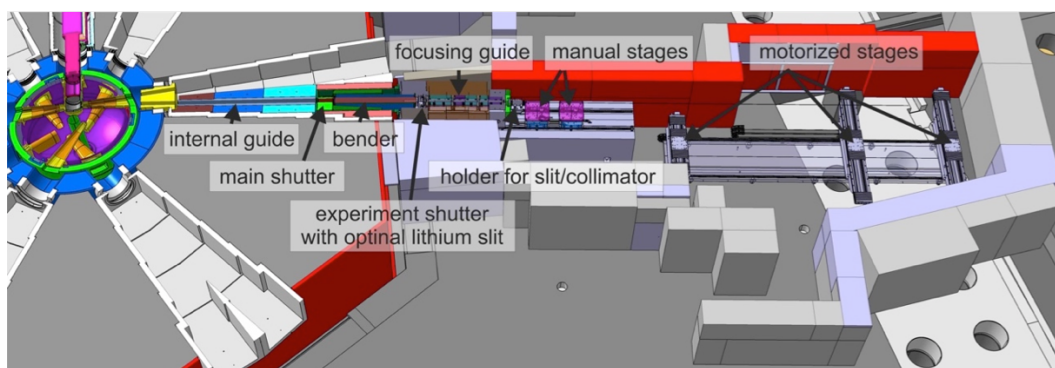


Figure 37: Illustration of the BOA beamline

The advantage of the BOA beamline for the measurements at hand is that it has a fast neutron beam as well as thermal/cold neutron beam. In addition the beams are separated in space. Figure 38 illustrates the separation.

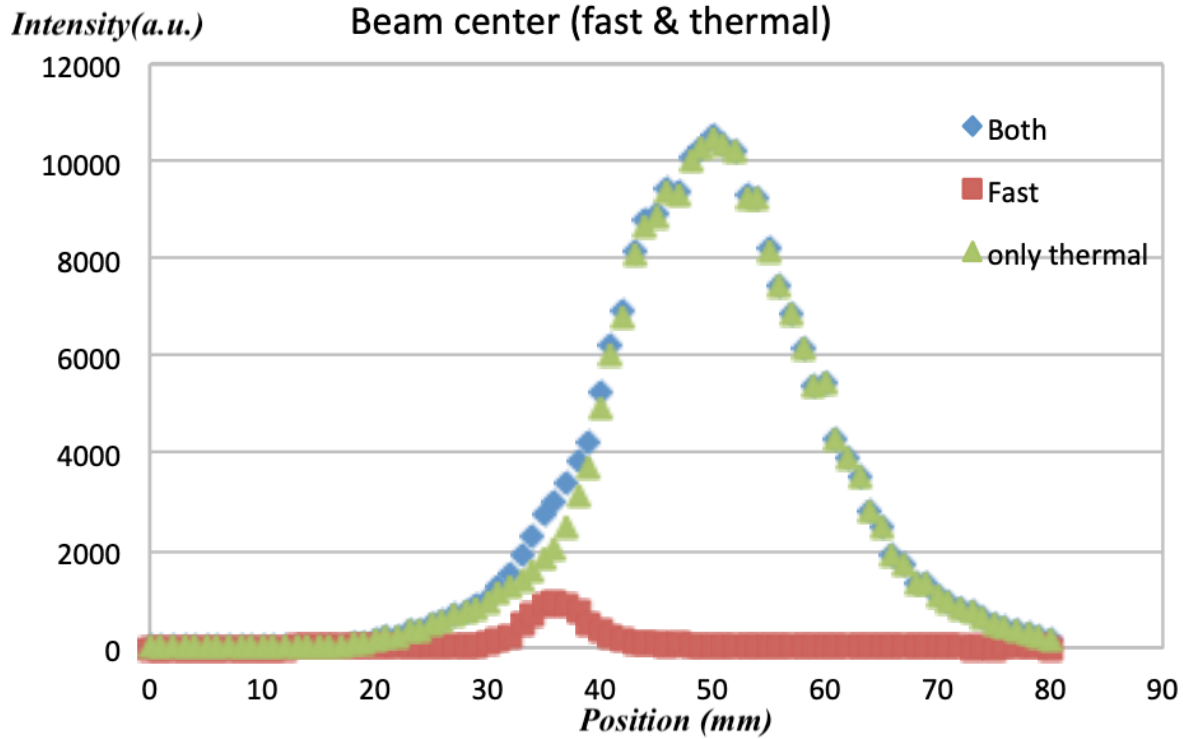


Figure 38: Fast and thermal neutron flux distributions, physically separated at the BOA beamline
For further details, please refer to the Deliverable D8.14 report.

The developed shielding box

A special shielding box (see figure Figure 39) was built which allows to measure/investigate the directional dependency of the neutron spectrum which includes the option to perform transmission measurements. Inside the box the BSS-system is positioned. The shielding box can be opened in any direction.

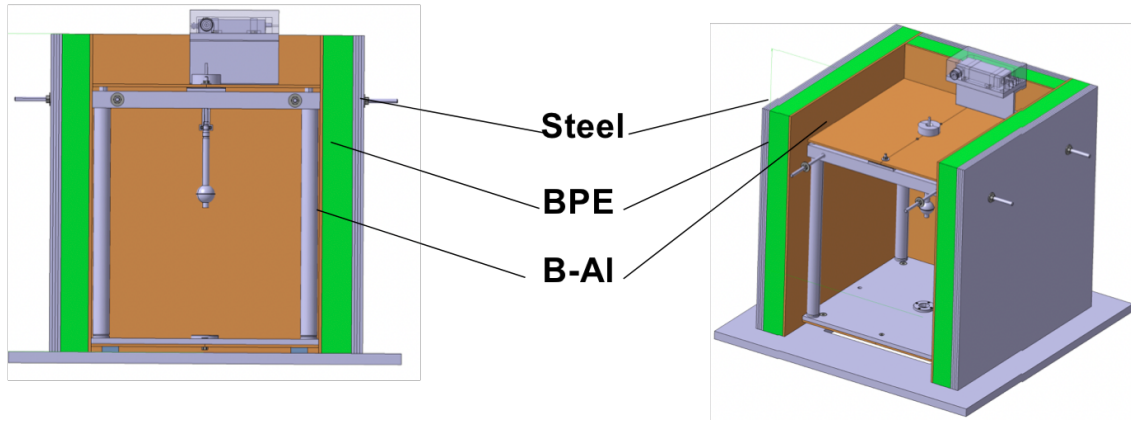


Figure 39: Shielding box for material investigations

The setup of the shielding box at the BOA beamline (see Figure 37) allows to vary a boron-layer (B-Al), borated polyethylene layer (BPE) and steel layers (several plates). The boron layer was 5 mm thick, the borated polyethylene 50 mm and the steel plates are 20 mm (4 times 5 mm). Figure 40 below show the shielding box set up at the BOA beamline for the study of fast neutrons from SINQ.

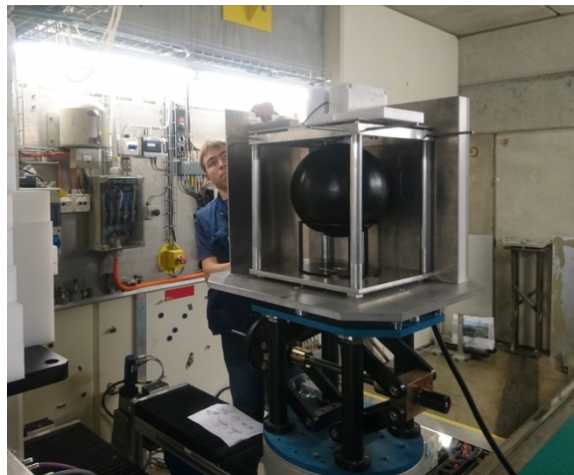


Figure 40: Transmission setup for the fast neutron beam at BOA

The transmission measurements

In a first setup the shielding layer sequence (shown in Figure 7) was investigated. The green layer is the BAl-layer. The orange layer is the borated polyethylene and the yellow layer is steel.

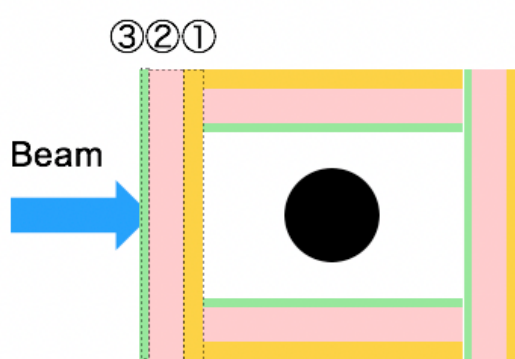


Figure 41: Transmission setup for the fast neutron beam at BOA

The measured results are shown in Figure 42 below. All three material layers reduce the fast neutron flux by a factor of three. The borated PE reduce strongly the epi- thermal neutron flux by factor of 25. The boron layer has only a 10-20 % effect. The conclusion is that 50 mm of borated polyethylene is a very effective shielding for the epi-thermal neutrons. The boron layer plus the borated PE layer reduce the thermal neutron flux by a factor of 40.

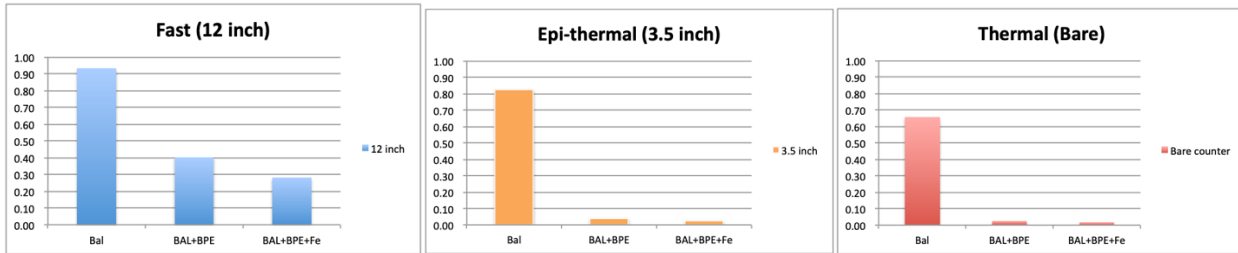


Figure 42: Fast, epi-thermal and thermal neutron transmission as measured using the BSS and shielding box at the BOA beamline in 3 different transmission configurations

Scattering from concrete

Another experiment was done to investigate the effect of backscattering from concrete environments/walls. To show this effect, a concrete sample was positioned in the beam and the detector was shielded as shown in Figure 43.

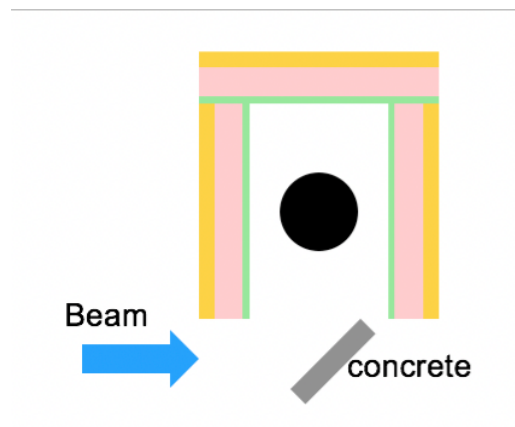


Figure 43: Concrete scattering setup

The concrete sample had a strong effect on the epi-thermal and thermal neutron flux. The epi-thermal neutron flux was increased by a factor 10 and the thermal neutron flux by a factor 8. A good shielding performance was measured by the use of the 5 mm BaI layer. The scattered epi-thermal and thermal neutrons were reduced strongly (see figure Figure 44). If the borated PE layer was added the background could be reduced by an additional factor 2 for epi-thermal neutrons and a factor 7 for the thermal neutrons.

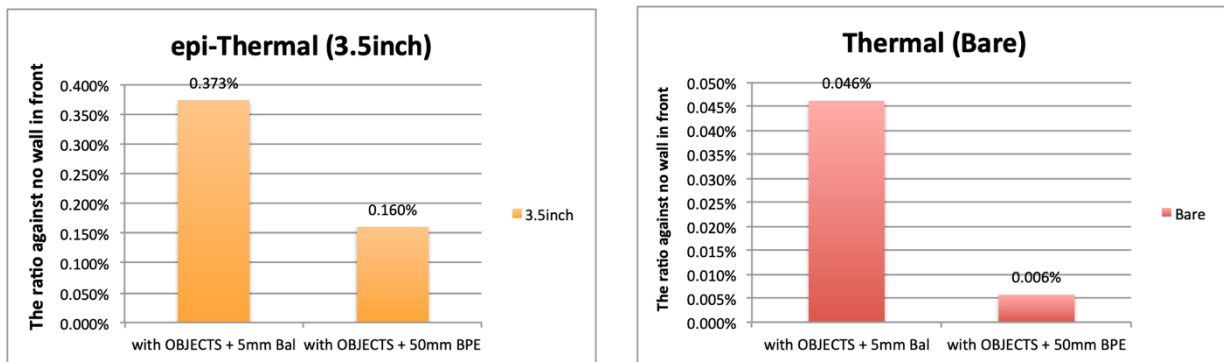


Figure 44: epi-thermal and thermal scattering reduction

For further details including specifics of a study of the background in the D8.14 experimental setting, please consult the D8.14 deliverable report.

Deliverable 8.16: Activation studies, radiation resistance

Introduction:

The radiation shielding properties of concretes and other structural materials of shielding, e.g. metals are well-studied and commonly simulated, unlike to the dose consequences of their neutron activation. In the context of D8.16, very detailed work was carried out on the neutron activation properties of three metal samples and three types of concretes, including the PE-B4C-concrete, developed in the European Spallation Source (ESS), see e.g. the first SINE2020 Periodic Report. The activity production in these samples was determined by neutron irradiation in the Budapest Research Reactor (BRR). PE-B4C-concrete showed significantly lower total activity concentration than its reference concrete. Further, the impact of concrete composition in activation production was demonstrated by activation simulations with the nominal composition - mostly limited to the bulk components - and multiple measured compositions of the concrete samples, using MCNPX and Cinder90. On this basis, realistic material cards were generated for activation simulations. The impact of concrete composition on decay gamma emission was also demonstrated in a maintenance case simulation of the ESS bunker. Decay gamma dose rates were found to be 29-72% higher with the use of the measurement-based input compositions, compared to the nominal ones, highlighting the importance of correct determination of trace elements in materials in relation to safety planning.

The D8.16 report presents a **very** complete and detailed study of the abovementioned studies, also available in the form of a manuscript submitted to NIM A.

Below we show a few highlights from the report, including photos of the studied samples, estimated decay curves for the 15 most important isotopes and finally comparisons between measured and simulated decay-profiles for Skanska, standard concrete and PE-B4C concrete.

Finally, decay gamma dose rate maps for the bunker of the BIFROST instrument have been simulated for the reference concrete parameters. Please consult the D8.16 report for further details.

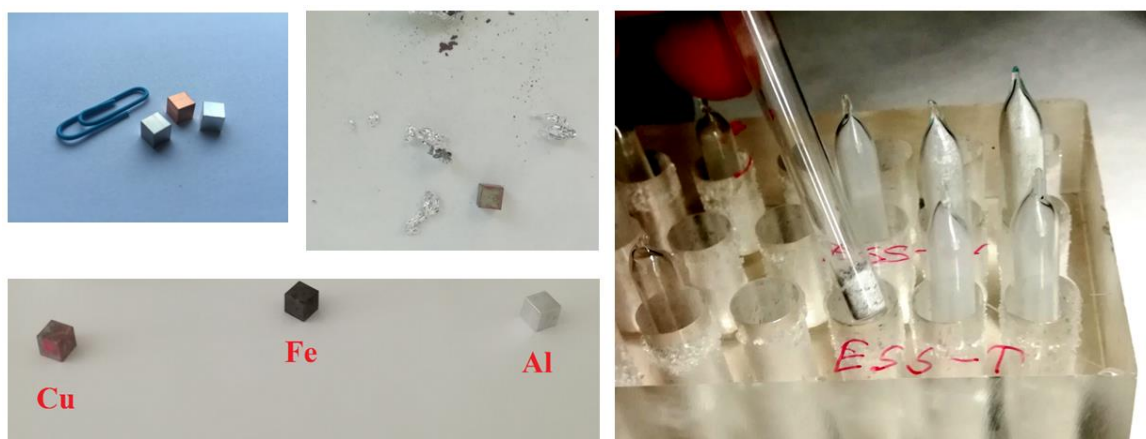


Figure 45: Initial (a) and irradiated metal samples (b, c), and encapsulated concrete samples prepared for irradiation (d).

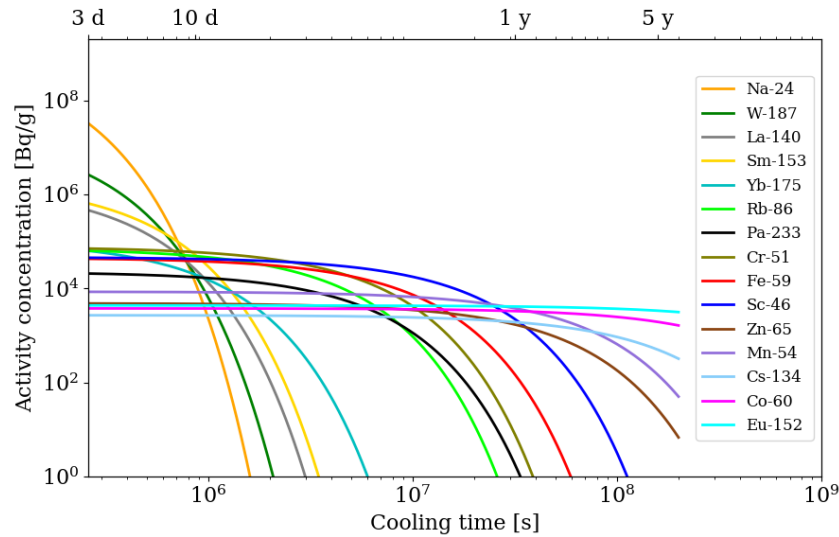


Figure 46: Decay curves of 15 key radioisotopes of PE-B4C-concrete after irradiation in the Fast channel, extrapolated from measured data.

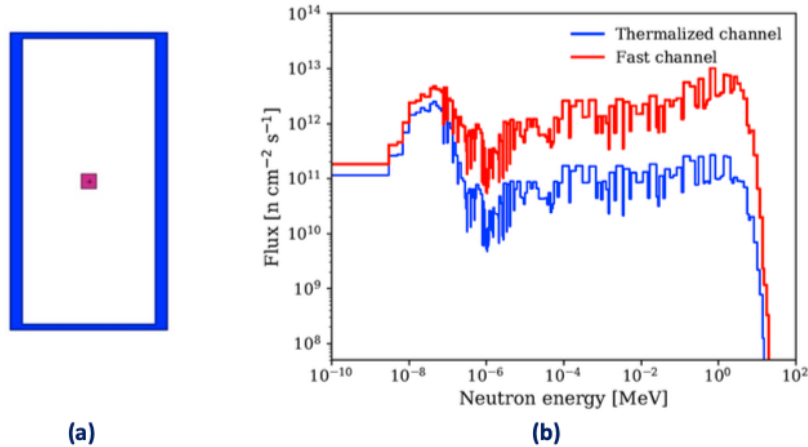


Figure 47: MCNP model for neutron irradiation simulations. (a) MCNP model for neutron irradiation in the vertical channels of the BRR. Pink: 5x5x5 mm³ cube sample, blue: 4 mm thick cylindrical aluminium container. The sample holder is filled with void. (b) Typical neutron flux in the vertical channels of the BRR, scaled with measured flux parameters from the monitor foils.

Periodic report template

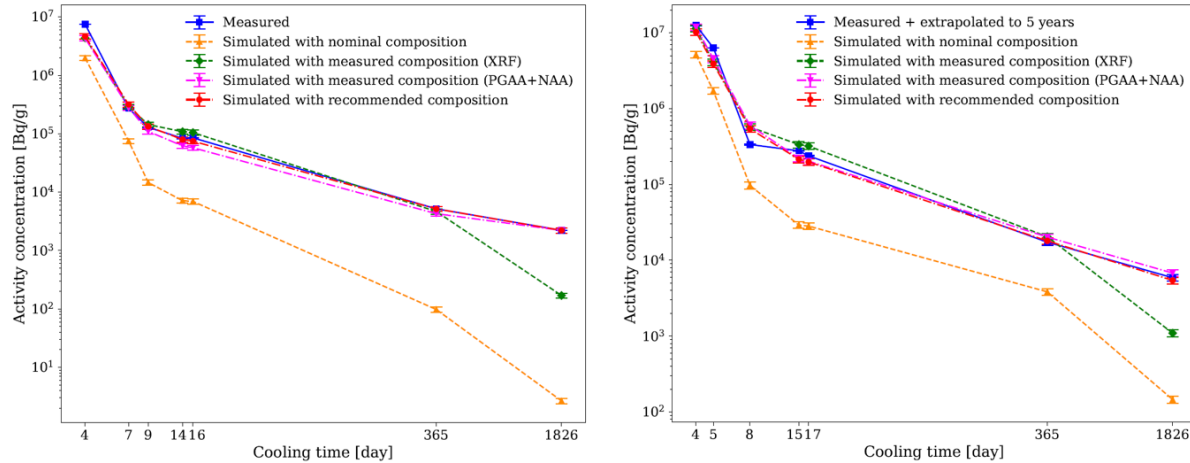


Figure 48: Measured decay profile of PE-B4C-concrete and simulated decay profiles with different initial compositions after irradiation in the Thermalized (a) and Fast channels (b). The statistical uncertainties are too small to be discernible.

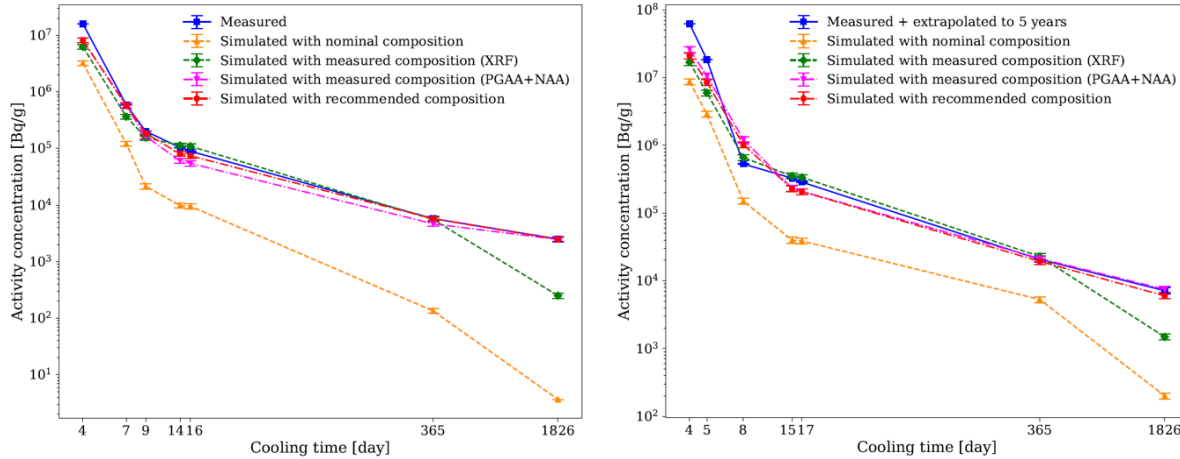


Figure 49: Measured decay profile of Reference concrete and simulated decay profiles with different initial compositions after irradiation in the Thermalized (a) and Fast channels (b). The statistical uncertainties are too small to be discernible.

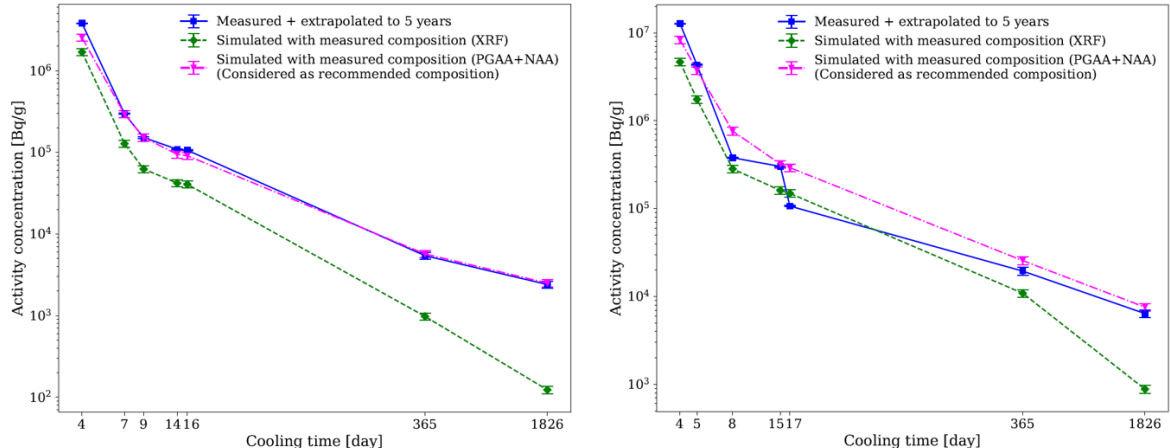


Figure 50: Measured decay profile of Skanska concrete and simulated decay profiles with different initial compositions after irradiation in the Thermalized (a) and Fast channels (b). The statistical uncertainties are too small to be discernible.

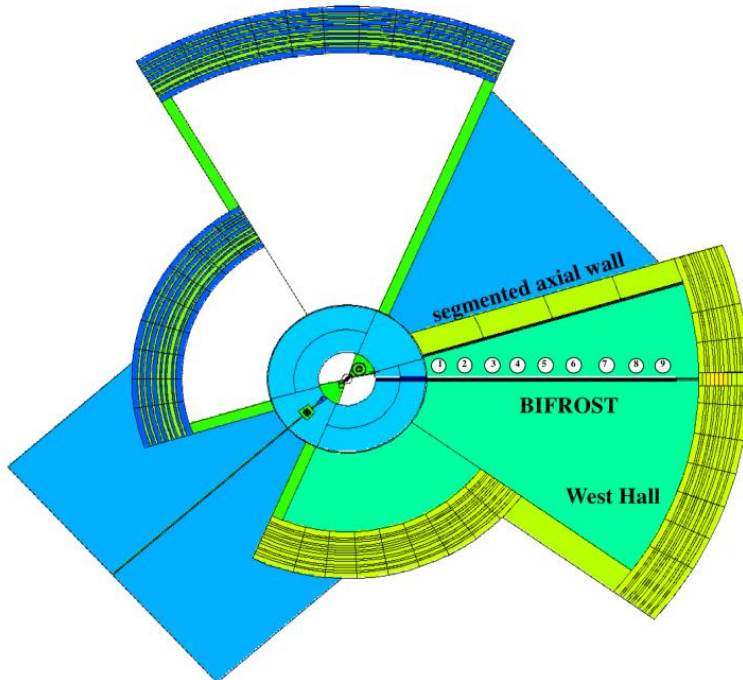


Figure 51: Overview of the MCNP model of the bunker complex. 1-9: 50 cm radius spheres along the neutron guide of the BIFROST instrument, marked areas for nominal comparison of decay-gamma dose rates.

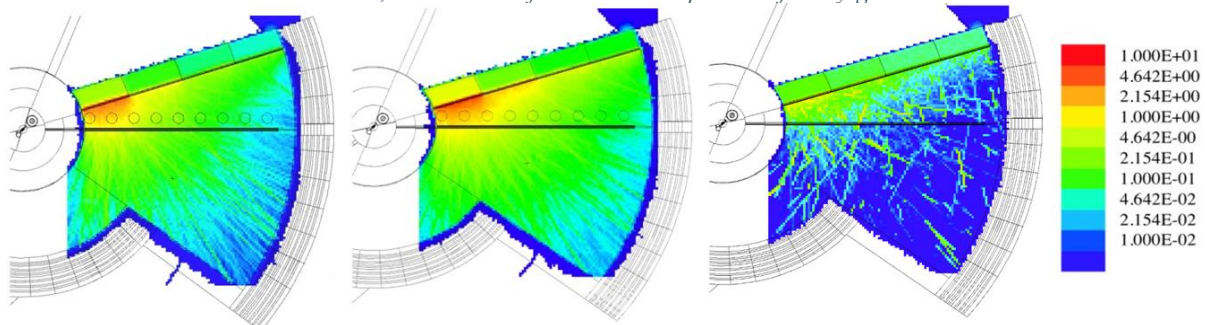


Figure 52: decay gamma dose rate maps [$\mu\text{Sv}/\text{h}$] of the West Hall after 3 days of cooling, with different compositions of the axial wall: nominal composition of the Reference concrete in (a), recommended composition of the Reference concrete in (b) and the currently used concrete for bunker simulations given in reference¹⁵

Deliverables 8.17 and 8.19: Investigation of different test samples

The experiments

The goal of task was to investigate shielding materials at different beam lines where the neutron spectra are different. We have chosen the beamlines ChipIR at ISIS and BOA beamline at PSI.

Experimental Setups at PSI and ISIS

As already outlined in the sections on D8.10 and D8.14, the BOA beamline has a fast neutron beam as well as thermal/cold beams available. As previously shown in Figure 38, the neutron spectra are physically separated at the beamline. After an un-folding procedure (see earlier Task

¹⁵ E. Zanini, L.; DiJulio, D.; Santoro, V.; Bentley, P.; Klinkby, “Neutronic design of the bunker wall and roof,” 2018.

8.2 reports from PSI), e.g. the fast neutron spectrum from SINQ can be estimated, see Figure 53 below.

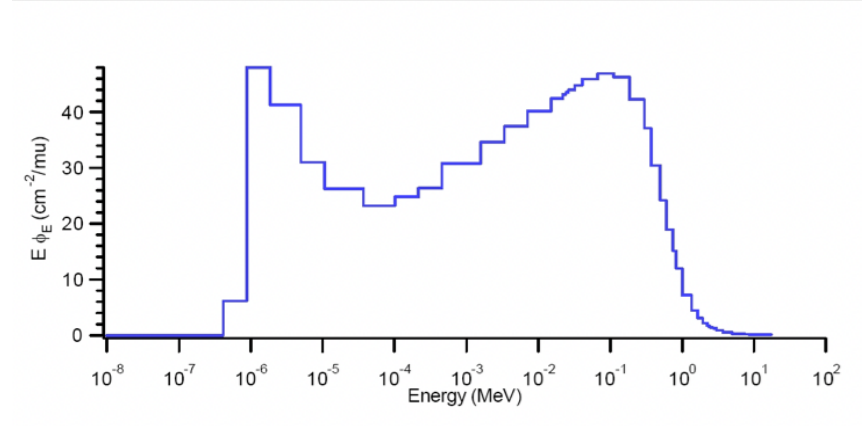


Figure 53: BOA – Fast neutron spectrum

In comparison the ChipIR beamline at ISIS has direct view to the moderator system (see Figure 54). The neutron spectrum looks completely different. It shows a strong fast neutron component in the range above 10 MeV.

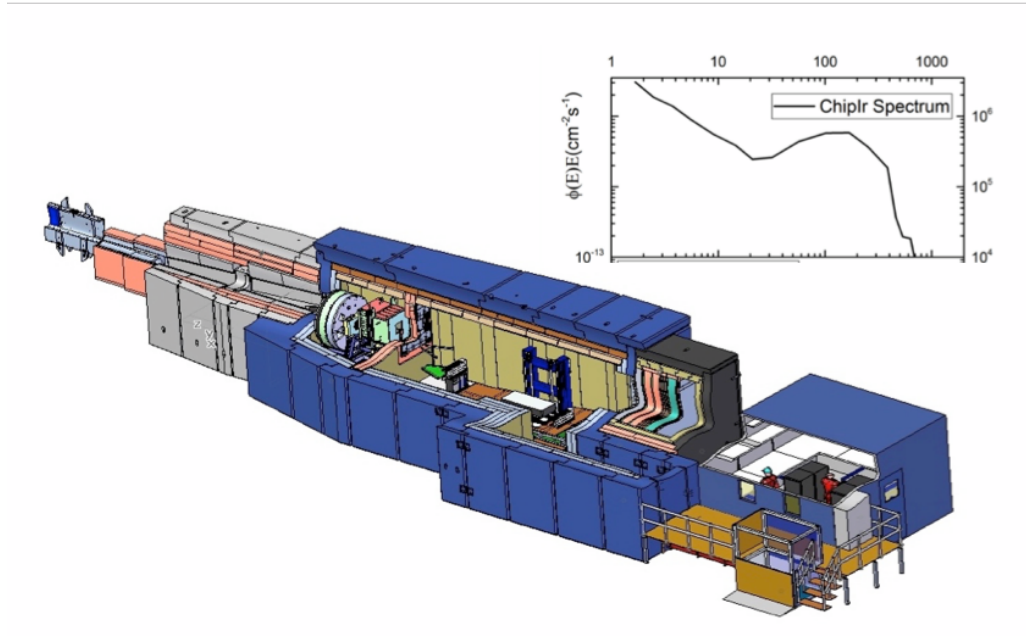


Figure 54: ChipIR beamline at ISIS with high neutron energy spectrum

Experimental result:

At both beamlines a borated mineral cast was measured. The sample thickness was 80 mm. Following the transmission measurements are shown. Furthermore tungsten (17 mm thick) and silicon (10 mm thick) samples were measured. The report D8.14 includes additional measurements from the BOA beamline.

Transmission measurements of mineral cast

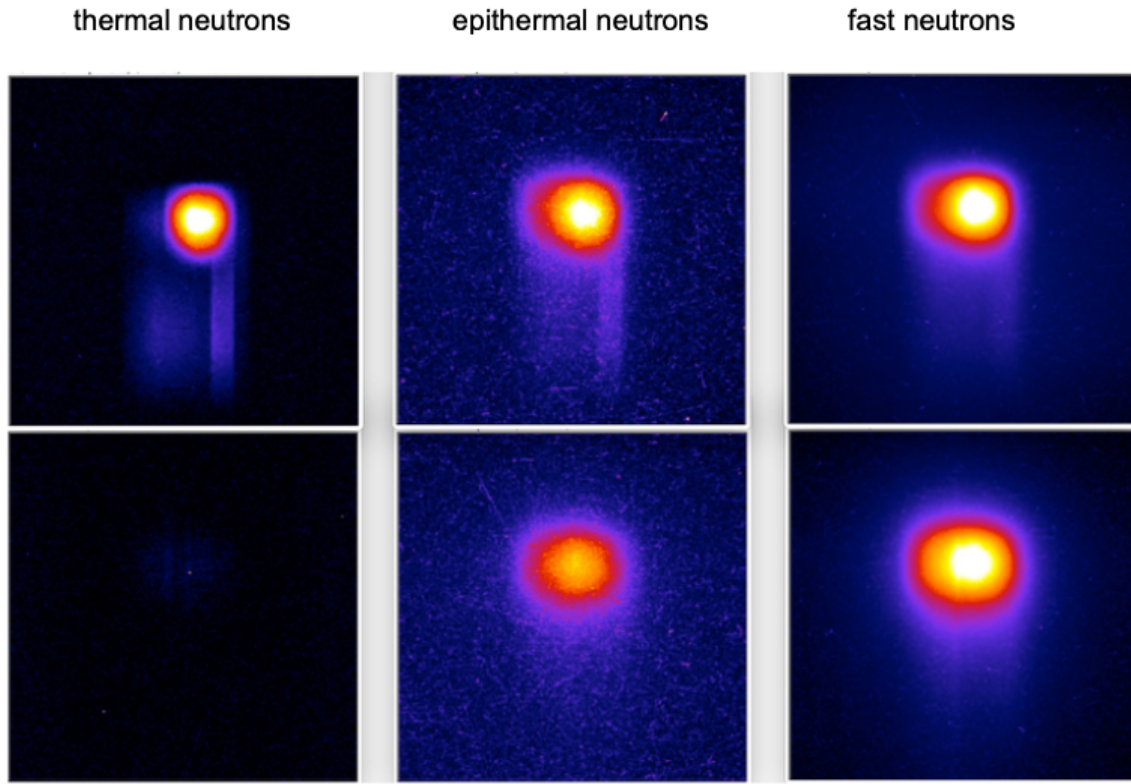


Figure 55: Transmission measurement for fast, epithermal and fast neutrons; first row – without sample; second raw – with sample

The thermal transmissions were measured at both beamlines BOA and ChipIR (first column of Figure 55). The transmission values are very closed. At ChipIR the measured thermal transmission was 2 percent. At the BOA beamline the value is a little bit lower (1 percent). That can be explained by the cold neutron spectrum at the BOA beam port. At ChipIR the thermal neutrons are more pronounced.

The epithermal transmission of the mineral cast was only measured at ChipIR (second column of Figure 55). The transmission was determined to be 63 %.

Finally the fast neutron transmission was measured (third column of Figure 55). Here we can observe the expected difference. At BOA, where the fast neutron spectrum is related to around 1 MeV neutrons, the transmission was measured with 58%. In comparison at the ChipIR beamline the transmission is lower. The measured value was 93 %.

Transmission measurements - Tungsten and Silicon sample

Tungsten is known as one of the best shielding materials for fast neutrons. For comparison reasons, tungsten test samples were measured at the ChipIR beamline. A steel sample (20 mm thick) was positioned above the tungsten to illustrate the strong shielding behaviour of tungsten.

Figure 56 shows the fast neutron transmission of tungsten. The tungsten sample was 17 mm thick. The measured transmission was 78 %. The steel sample has 95 % transmission.

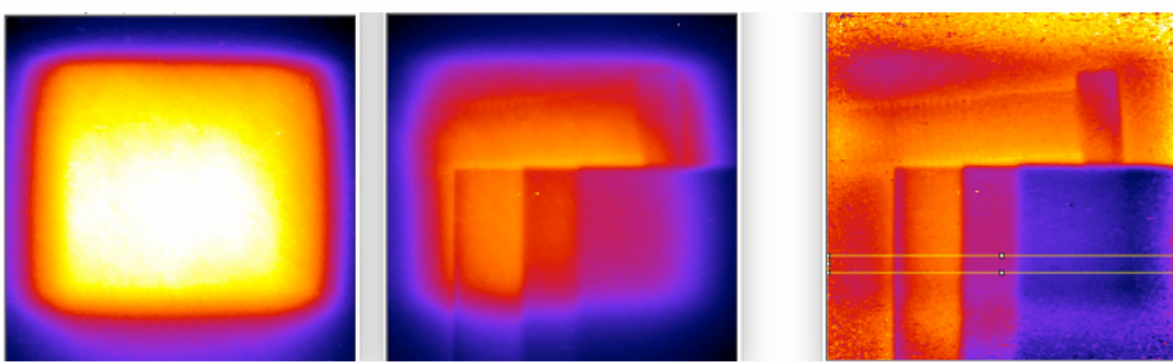


Figure 56: Tungsten transmission by 3 plates – each 17 mm thick; on the top the steel sample is positioned. Left: without sample; middle: transmission measurement; right: corrected/substracted data

The mineral cast shows strong shielding characteristics in the thermal neutron range. A Silicon sample was chosen to demonstrate the difference in shielding power. Figure 57 shows the thermal transmission of Silicon at the ChipIR beamline. The transmission is more than 85 %.

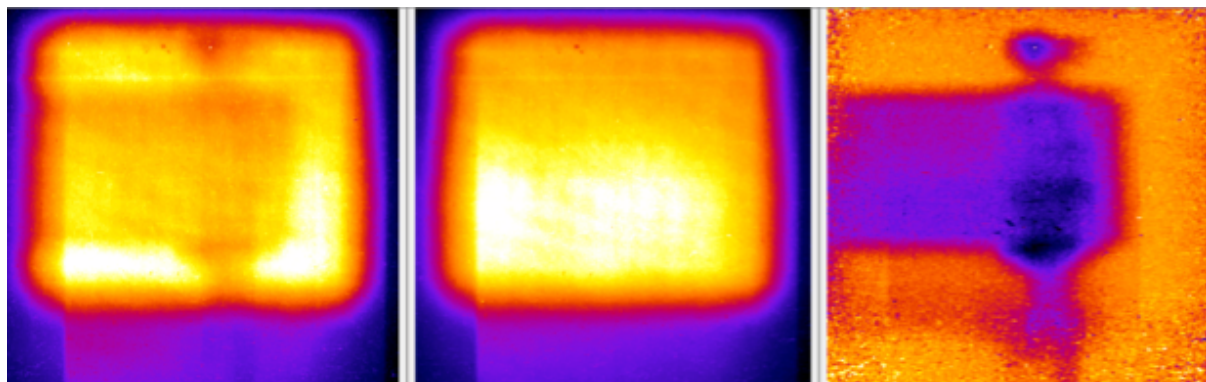


Figure 57: Silicon transmission - 10 mm thick; Left: measurement with sample; middle: measurement without sample; right: corrected/substracted data

Deliverable 8.19: Validation of the measurements by Monte Carlo Simulation

Abstract

In previous deliverable D8.5, a database of neutron transmission through a number of materials was created. Here, we make an example of how to employ said database to a shielding sizing and material choice. In this particular case, the Chopper Pit of the MIRACLES BeamLine at ESS is used. The neutron flux and spectrum resulting from the interaction of the beam with the closed chopper is used as an input, and different configurations are calculated and compared, with a brief discussion about the calculation times and the possibilities this methodology opens.

Introduction

Neutron shielding in any complex geometry in general, and in beamlines in particular is a computational heavy task, that requiring CPU times in the order of thousands of CPU-hours per case studied. If studying a variety of shielding configurations, specially materials, there is also a significant personal work required. Modification of models in typical Monte Carlo codes like

Periodic report template

MCNP are also remarkably error-prone, which, in turn, typically lead to more corrections and more worktime used up. For this reason, usually very few configurations are tried out, and the modifications are kept as simple as possible.

For this reason, a complementary method to explore new shielding configurations, is of interest for design. This method is focused on speed and ease of calculation, even if the results can only be taken comparatively. Previously, in D8.3, a transmission factor library was compiled for a number of materials. The idea behind those transmission factors is that, for a monoenergetic incident neutron beam with intensity Φ , and energy E_0 the output spectrum can be defined as $\Phi'(E_i) = A(E_i, E_0)$, where $A(E_i, E_0)$ is the transmission factor corresponding to these energies. We can thus arrange those factors in a square matrix A , so that, for any entering spectrum, we can calculate the outlet spectrum as: $\Phi'(E) = A \cdot \Phi(E)$. This calculation is effectively immediate on any personal computer, thus allowing the shielding designer to try out as many configurations as he wishes without any access to High Performance Computer whatsoever.

In this work, we have tried to apply this method as well as traditional Monte Carlo calculation to the experiments performed at the ChipIr instrument of the ISIS Second Target Station (see Deliverable report D8.17 and related section above), and the results are discussed.

For full details, please consult deliverable report D8.19.

Illustrations of the MCNP model used:

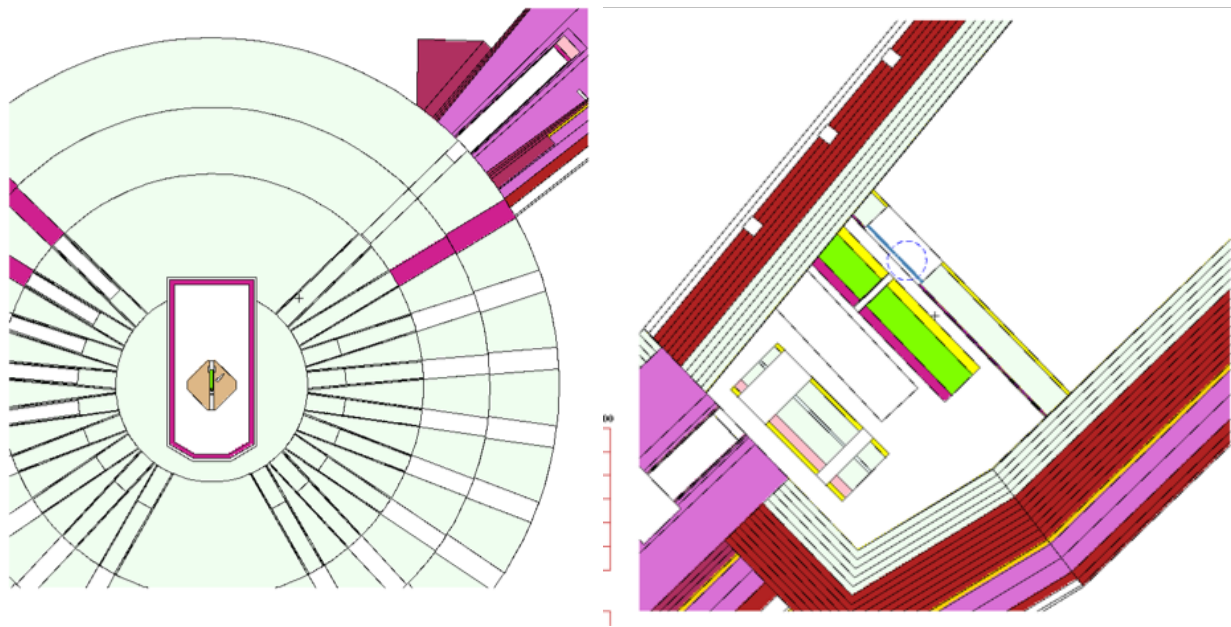


Figure 58: Left: General view of the ISIS-TS2 model. Right: Overview of the Chipir experimental area with modified tallies and drum.

A Global Variance Reduction Weight Window was generated for this model, using a MAGIC¹⁶ method. The minimum importance value chosen was 1E-5.

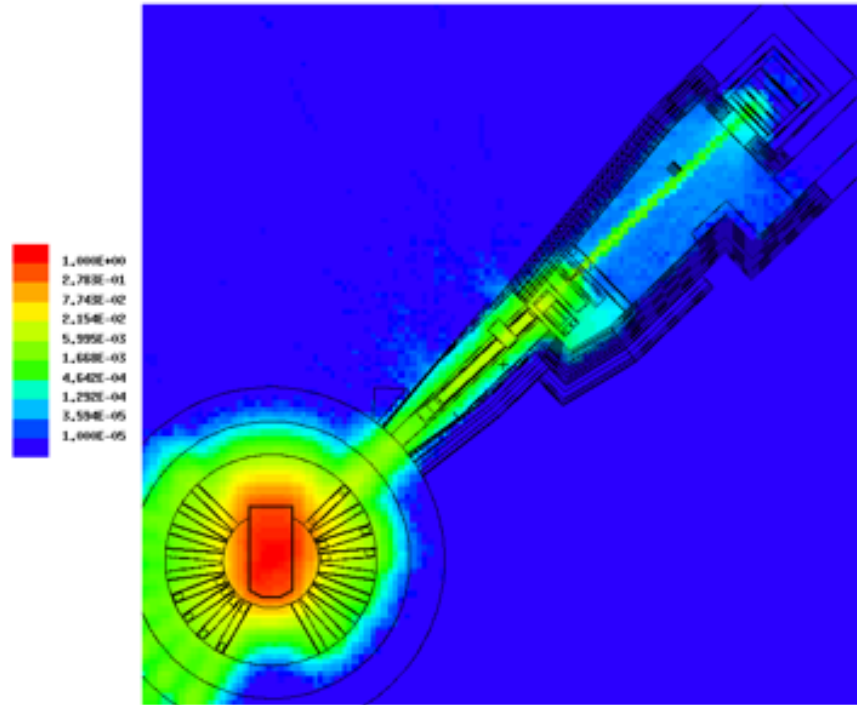


Figure 59: Weight window used for calculations

As an initial check to the model and variance reduction, the jaws opening was set to 70x70mm, and the spectrum in the point detector $>0.1\text{MeV}$ was calculated and compared to known data .The result, normalized to $5\text{E}+06 \text{n/cm}^2\text{s}^{-1}$ measured over 10 MeV, is plotted in Figure 60 on the right, with the comparison with reference ¹⁷ to the left .

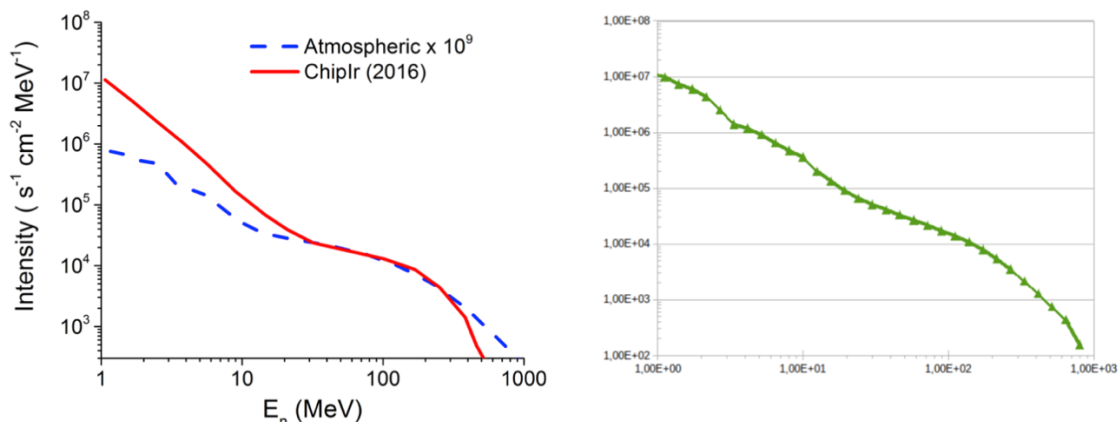


Figure 60: Measured spectrum at ChipIr from Reference 17 (left) and results from Monte Carlo model (right)

¹⁶ Davis, Andrew Alexander and Andrew Turner. "APPLICATION OF NOVEL GLOBAL VARIANCE REDUCTION METHODS TO FUSION RADIATION TRANSPORT PROBLEMS." (2011).

¹⁷ Carlo Cazzaniga and Christopher D. Frost, IOP Conf. Series: Journal of Physics: Conf. Series 1021 (2018) 012037

The results show reasonable agreement between both datasets. At the highest energies, near incident proton energy, the Monte Carlo simulation overestimate the spectrum somewhat, as an effect of using point detectors, which do not accurately describe the anisotropy of the physics at those energies. This result shows that the model is a good description of the actual instrument.

Incident 10x10mm beam

As the experimental campaign was performed using this aperture, we first modified the jaws until the beam shape matched the 10x10mm beam. This determines the incident beam on the sample, and serves as a comparison to the experimental data. A mesh tally was set up with 1mm mesh size to track the results, and a separate run was used for the fast neutrons, using energy cutoff to accelerate the calculations and improve statistic. Figure 61 shows the incident beam for the three energy groups defined in the table below.

Energy group	Min energy	Max energy
Thermal	1 meV	400 meV
Epithermal	400 meV	800 keV
Fast	800 keV	800 MeV

Table: Neutron energy groups

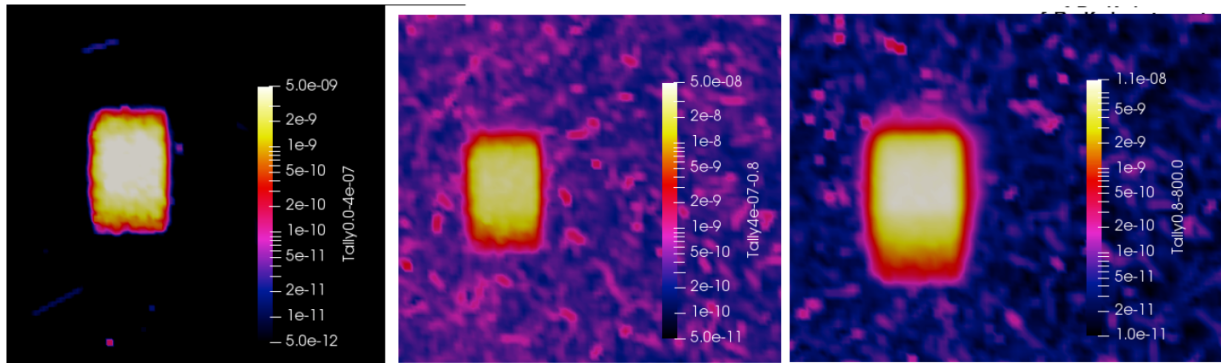


Figure 61: Incident beam for Thermal (left) Epithermal (mid) and fast (right) neutrons

A few conclusions can be derived from these results and their comparisons with the incident beams from the experimental campaign:

- The shape of the beam seems slightly taller and less rounded than the experiments. This is likely a result of the adjustment of the jaws.
- The halo around the beam is clearly visible but significantly smaller in the simulations. Placement of the samples in the model and in reality, could influence this result. Importantly, the simulations agree with the experiment in that the relative size of the halo increases with the neutron energy.

- While the simulation suffers from significant noise in the statistic, it successfully shows that the background around the beam is insignificant for thermal neutrons, and slightly higher from epithermal than from fast neutrons.

Overall, and especially considering the limitations and simplifications used in the geometry, the Monte Carlo calculation achieve a rather positive approximation to the experimental measurements from D8.17. For further details, please refer to the deliverable report D8.19.

Task 8.3: Compact Instrumentation for Larmor Labelling applications at the ESS (Responsible: TU-Delft with observers: DTU, STFC, MTA-EK and ESS)

Larmor labelling is widely used to increase the resolution of neutron scattering both in energy (Neutron Spin Echo spectroscopy¹⁸) and momentum transfer (Spin Echo SANS¹⁹, Larmor diffraction²⁰). Since these techniques do not require highly monochromatized and collimated neutron beams they do not trade resolution for neutron flux. However, the effective neutron count rate is effectively reduced because of the use of polarised neutron beams and because the Larmor precession areas cannot be combined with neutron guides. Furthermore, most existing instruments are relatively long, due to homogeneity requirements for the precession areas. This in fact collimates the beam and significantly reduces the neutron flux.

Deliverable 8.15: Recommendations for ESS instruments, possibly also with the help of simulations

1. Introduction

Larmor labelling uses the precession phase of the neutron beam polarization P around a magnetic field B to directly measure the energy or the momentum transfer at the sample. Thus, the performance of the instruments is a function of the homogeneity and geometry of the magnetic field over the areas, where the precession takes place. In our previous deliverable²¹ we showed that the important parameter for the design of Larmor labelling instrumentation is the magnetic field integral $\int B(l) dl$, taken over all possible trajectories of the neutron beam. Ideally this integral should be the same for all trajectories for (NSE) or vary in a well-defined and controlled way (for SESANS). The stringent requirements on the magnetic field homogeneity lead to relatively long instruments, a design that ultimately collimates the neutron beam and reduces the neutron flux.

The aim of this deliverable was to investigate the effect of the ESS flat pancake moderators on the design of Larmor labelling instruments. These moderators deliver high intensity neutron beams, which are confined in a small cross-section and are well-adapted to small samples and compact instrumentation. On the basis of extensive analytical calculations and simulations²¹ we have shown that the geometry of the ESS neutron beams improves significantly the performance of Larmor labelling setups. However, we found that the overall dimensions of the resulting

¹⁸ F. Mezei; Neutron Spin Echo, Lecture Notes in Physics, **128**, Springer, (1980), 3.

Mezei, F.; Pappas, C.; Gutberlet, T; Lecture Notes in Physics, **601**; Springer (2003).

¹⁹ M.T. Rekveldt; *Nucl. Instrum. Methods Phys. Res. B*, **114** (1996) 366.

²⁰ M.T. Rekveldt; W. Kraan; T. Keller; *J. Appl. Crystallogr.*, **35** (2002) 28.

²¹ Deliverable report Nr. D8.7

instruments do not shrink substantially. In the following we provide recommendations for the two compact configurations investigated: a Neutron Spin Echo (NSE) Spectrometer and a SEMSANS add-on for SANS and Imaging.

A Compact Neutron Spin Echo Spectrometer

The magnetic field configuration considered is schematically shown in Fig. 1. This is the first arm of an NSE spectrometer, where the neutron beam exits a polarizing neutron guide. The precessions start at the $\pi/2$ flipper, which is positioned at a distance a_1 from the blue rectangular shape representing the main coil of length L and radius R . A π flipper between the main coil and the sample, at a distance a_2 from the end of the coil, marks the reversal point of the precessions. Additional coils, modeled by current loops, lower the magnetic field at the positions of the $\pi/2$ and π -flippers. In the calculations the efficiency of the flippers was assumed to be 100% and thus their intrinsic adiabaticity was ignored.

The results^{21,22} show that there is a clear gain with the “pancake moderator” beams. Indeed, rectangular beam cross-sections with a height over width ratio, e.g. 1:4, that mimic the ESS “pancake moderator” beams lead to the best results, and improve the homogeneity of the magnetic field integrals by at least 30 %. On the other hand, because relative inhomogeneities become worse for shorter coils, in order to reach high resolution, i.e. long Fourier times, the length of the instruments cannot be reduced. Consequently, NSE spectrometers will perform better at the ESS, as the required magnetic field integral corrections (through Fresnel coils) will be weaker, but they will not be more compact than e.g. at the ILL or FRM2.

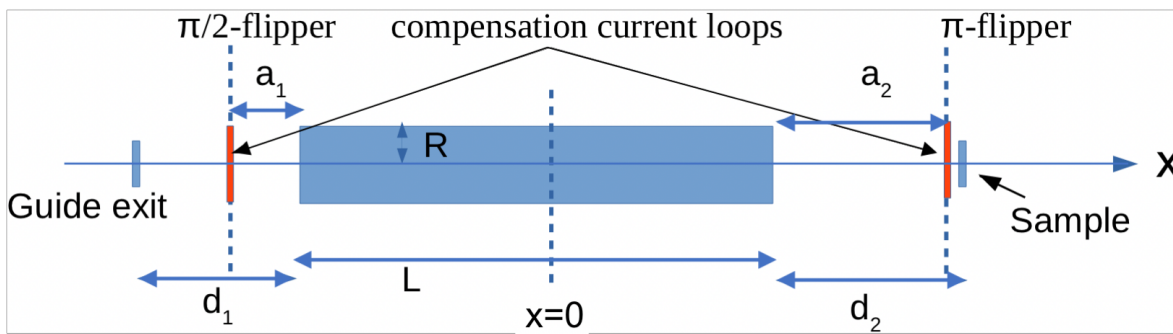


Figure 62: Schematic representation of the configuration considered for the first arm of a NSE spectrometer. The layout is characterized by the lengths L , a_1 , a_2 and R . The blue rectangular area represents the main precession coil.

B Compact SEMSANS add-on for SANS and Imaging.

The configuration used for the magnetic field calculations is schematically shown in Fig. 2. The setup had an overall length of 3.1 m and reproduced a test arrangement used for an experiment at the HZB, on the V20 ESS test beamline²³. The magnetic field configuration has been calculated and optimised using the Infolytica MagNet software. All major components were included in the model, such as the guide field, Vcoils, DC magnets, field stepper. The dimensions were chosen such as to correspond to a standard setup and may be easily scaled to investigate the effect of a compact beam size.

²² A. Kusmin and C. Pappas, to be published at the Journal of Neutron Research

²³ J. Plomp et al. to be published

The results show that one can change the dimensions while keeping the optimised [x,z,y] ratios for the components. For the setup investigated, this implies that when considering the beam geometry of the ESS pancake moderators, the overall length can be reduced from 3.1 m to 1.1 m, which can be considered as the minimal length for such an add-on setup. Such a compact design could be easily implemented as an add-on. It could be installed and removed, according to the experimental requirements and would substantially extend the capabilities of the ESS. A possible host instrument would be the polarised neutron SANS, SKADI, where the add-on would allow simultaneously SANS and SEMSANS measurements. Another host instrument candidate is the neutron imaging instrument ODIN, where the add-on could be used for high resolution dark field imaging²⁴.

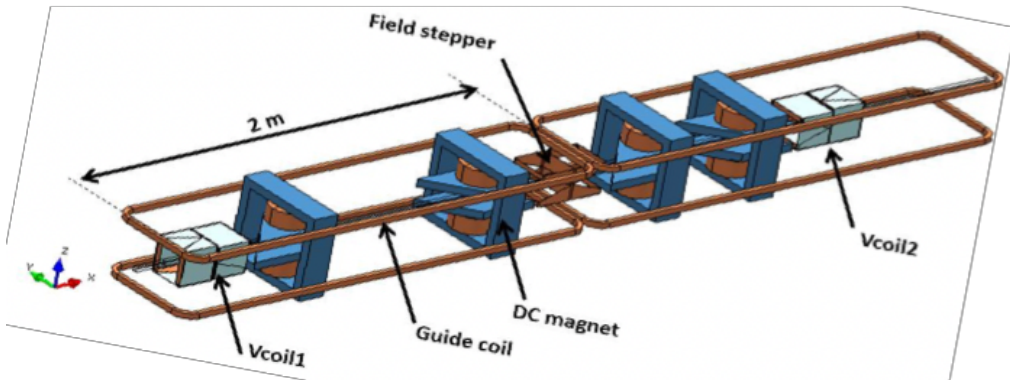


Figure 63: Schematic drawing of SEMSANS arrangement considered for the magnetic field calculations. The white boxes illustrate the Vcoils, which act as $\pi/2$ flippers, the blue components are DC magnets with parallelogram shaped pole shoes, the central coil is a field stepper. The long upper and lower create a homogenous magnetic field, which guides the beam polarisation.

Date	Meeting/workshop	Location	Who participated
22-25/10-18	NOBUGS 2018	BNL, Long Island NY, USA	WP leader
28/05/2019	WP meeting	Bilbao, SPAIN	WP team, see participant list in minutes
28-29/05/2019	3 rd General Assembly	Bilbao, SPAIN	WP team, see participant list in minutes
29/6-19	ISTSII2019 workshop	Skt Petersburg, Russia	WP team, see participant list in minutes
30/6-5/7-19	ECNS2019	Skt Petersburg, Russia	WP team

²⁴ M. Strobl, et al. *Nature Scientific Reports* **5**, 16576 (2015).